

REACH TO GRASP MOTION CAPTURING SYSTEM
USING SINGLE CAMERA

SAHAWATCHARA THONGPRASAN

A THESIS SUBMITTED IN FULFILLMENT
OF THE REQUIREMENT FOR THE DEGREE OF
MASTER OF ENGINEERING IN ELECTRICAL AND COMPUTER ENGINEERING
SCHOOL OF ENGINEERING

KING MONGKUT'S INSTITUTE OF TECHNOLOGY LADKRABANG

2023

KMITL-2024-EN-M- 317-286

This material is reserved for educational use only, not allowed for commercial use.

Forbidden to modify the content, and cite the document when use.



COPYRIGHT 2023

SCHOOL OF ENGINEERING

KING MONGKUT'S INSTITUTE OF TECHNOLOGY LADKRABANG

This material is reserved for educational use only, not allowed for commercial use.

Forbidden to modify the content, and cite the document when use.

Thesis	Reach-to-Grasp Motion Capturing System Using Single Camera
Student	Mr. Sahawatchara Thongprasan
Student ID.	64601147
Degree	Master of Engineering
Program	Electrical and Computer Engineering
Year	2023
Thesis Advisor	Asst. Prof. Dr. Suradej Tretriluxana

ABSTRACT

Evaluating human motion is crucial for effective physical therapy interventions. This study introduces an innovative system for tracking the motion of the human upper extremity, specifically focusing on functional analysis. Utilizing a single smartphone camera as the core of an optical motion capture system, we captured Reach-to-Grasp (RTG) movements of subjects in a seated position. Image analysis techniques were employed to identify MediaPipe Hand and the Perspective-n-Point (PnP) algorithm located on selected anatomical landmarks of the hand. Through a straightforward camera calibration method, we acquired the 3D coordinates of hand movements. We then calculated two key clinical metrics: grasp aperture and hand transport velocity. These metrics were subsequently compared with data gathered simultaneously from a high-precision Electromagnetic Motion (EM) tracking system. The patterns of results from both systems showed a high degree of correlation. We are currently refining our algorithms based on clinician feedback. This system holds potential for aiding physical therapists in assessing patient movement within clinical environments.

ACKNOWLEDGEMENTS

I would like to express my deepest gratitude to my advisor, Asst. Prof. Dr. Suradej Tretriluxana, for his invaluable guidance, unwavering support, and mentorship throughout the course of this research. His expertise and insights have been instrumental in shaping this thesis, and I am profoundly thankful for the opportunity to learn under his tutelage.

Authors would like to acknowledge Ms.Rukshana Poudel and Ms.Narana Onsri, graduate students at the Motor Control and Neural Plasticity Laboratory (MCNL), faculty of physical therapy, Mahidol university for their assistance with the data collection I would like to extend my sincere appreciation to Assoc Prof Dr.Jarugool Tretriluxana as the Director of Motor Control and Neural Plasticity Laboratory (MCNL), faculty of Physical Therapy, Mahidol University for the lab equipment and invaluable advices.

I am also grateful to the faculty and staff at King Mongkut's Institute of Technology Ladkrabang (KMITL) for providing an enriching academic environment that has facilitated my growth as a researcher. The resources and facilities at KMITL have been indispensable in the completion of this work.

Last but not least, I would like to thank my family and friends for their constant encouragement and emotional support. Their belief in me has been a source of strength and inspiration.

Sahawatchara Thongprasan

TABLE OF CONTENTS

	Page
ABSTRACT	I
ACKNOWLEDGEMENTS	II
TABLE OF CONTENTS	III
LIST OF FIGURES	V
1 Introduction	1
1.1 Background	1
1.2 Objective	3
1.3 Hypothesis	3
1.4 Scope of study	4
2 Theory	5
2.1 Camera calibration	5
2.2 Motion Capture Systems	15
2.3 Mediapipe	15
2.3.1 Detecting and Pose estimation	16
2.3.2 Tracking	22
2.4 PnP algorithm	23
3 Research methods	29
3.1 Camera calibration procedure	29
3.2 Preparation for experiment	32
3.3 Compute 3D coordinates	35
3.4 Compare result from Electromagnetic and Single camera	37

TABLE OF CONTENTS (CONTINUE)

	Page
4 Result and Discussion	38
4.1 Aperture	38
4.2 Height	39
5 Conclusion	40
5.1 Conclusion	40
5.2 Future work	40
Appendix	
Table 1 Result from trial1	B
Table 2 Result from trial2	D
Table 3 Result from trial3	F
Table 4 Result from trial4	H
Table 5 Result from trial5	J
REFERENCES	K
BIOGRAPHY	M

LIST OF FIGURES

	Page
Figure 1 2D to 3D chessboard	6
Figure 2 chessboard multiple view	15
Figure 3 Pose estimation by Mediapipe	17
Figure 4 Palm detector model architecture (left). Hand landmark model architecture (right) .	18
Figure 5 Examples of datasets. (Top): Annotated realworld images. (Bottom): Rendered synthetic hand images.	22
Figure 6 Tracking by Mediapipe	23
Figure 7 Perspective-n-Point (PnP) algorithm	29
Figure 8 Chessboard for camera calibration	32
Figure 9 Setup of experiment	33
Figure 10 The locations of markers for motion capture system	34
Figure 11 Reach to Grasp motion	35
Figure 12 Compute 3D coordinate	37
Figure 13 Aperture from three system	40

Chapter 1

Introduction

1.1 Background

The assessment of human movement is a critical aspect of physical therapy management. Understanding and analyzing the function of the upper extremity, particularly the Reach-to-Grasp (RTG) movement, is essential for evaluating a patient's motor skills, recovery progress, and the effectiveness of therapeutic interventions. Traditional methods of assessing these movements often involve high-cost equipment, such as Electromagnetic Motion (EM) tracking systems, which may not be readily available in all clinical settings. Furthermore, these systems may require complex setup and calibration processes.

A significant application of Motioncapture is its utilization in the healthcare sector, specifically in physical therapy, where it is employed to monitor, analyze, and evaluate human movement [2-3, 8-13]. The system is designed to capture either the entire body or specific parts during various activities. In the context of this work, our focus is primarily on the functions of the upper extremity, with a particular emphasis on the Reach-to-Grasp movement.

The Reach-to-Grasp (RTG) movement is a commonly performed activity in human upper limb movement [1]. Deficits in this function often necessitate physical therapy and are typically the aftermath of neurological conditions such as stroke and Parkinson's disease [2, 8-13]. In a clinical setting, physical therapists analyze the RTG movement through observation or clinical tools [2]. To acquire quantitative measures, the use of a motion tracking system is essential [3]. In this research, the Electromagnetic Motion (EM) tracking system, known for its high resolution and ease of use, is the standard instrument [4-7]. This system delivers the 3D coordinates of sensors positioned on anatomical landmarks at the millimeter scale [5]. However, EM's high cost and lack of portability prevent its use in Telemedicine.

Telemedicine is the use of digital technology to provide medical care and consultations remotely. It is crucial for reaching patients in remote or underserved areas, improving access to healthcare, reducing the need for travel, and enabling ongoing management of chronic conditions. However, Electromagnetic Motion (EM) tracking systems are not suitable for telemedicine because they are expensive and not portable. These systems need costly equipment and complicated setups, making them impractical for use outside of specialized clinics. Computer vision technologies, on the other hand, are more affordable and portable. They allow for remote assessment and monitoring of patient movements without the need for bulky and expensive equipment, making them ideal for telemedicine[15,16].

Computer vision in motion capture can use either multi-camera or single-camera setups. Multi-camera systems provide high accuracy and detailed 3D motion data, which is great for complex motion analysis. However, they are expensive, require extensive setup, and are not portable[17], limiting their use in telemedicine. On the other hand, single camera systems are more affordable and portable, making them ideal for remote healthcare. While they may not be as precise as multi-camera systems, their convenience and lower cost are significant benefits. A single smartphone camera is especially useful for telemedicine because it is cheap and widely available[18]. Using MediaPipe, a machine learning framework by Google, a single smartphone camera can effectively detect and analyze hand movements. MediaPipe Hand can identify hand keypoints and estimate 3D positions, offering a practical and accessible solution for remote patient monitoring.

MediaPipe Hand is a machine learning framework developed by Google[19] that specializes in hand detecting and pose estimation. It is designed to identify 21 3D hand keypoints, which include the positions of individual finger joints, the palm, and the wrist. The framework is capable of handling both single and multiple hands within the same frame. MediaPipe Hands utilizes a two-step process: first, it employs a palm detector model to identify the location of a hand in the image, and then it applies a hand landmark model to estimate the 21 3D keypoints. This technology is

widely used in various applications, from augmented reality to human-computer interaction, and is praised for its accuracy and robustness.

In a single camera setup, such as the one used by MediaPipe Hand, accurately estimating the depth (Z-axis) of fingertips can be challenging. While MediaPipe provides 3D keypoints, the Z-axis information is generally normalized and relative, not an absolute measure of depth. Depth estimation in this context often relies on cues like object size and perspective, along with previously learned data. Although these methods can offer a reasonable approximation of depth, they may not be as precise as specialized depth-sensing cameras or multi-camera configurations. Therefore, for applications requiring critical depth information, additional hardware or techniques are often recommended.

The Perspective-n-Point (PnP) algorithm[20] is a well-established technique used for solving the pose estimation problem, which involves determining the position and orientation of an object—in this case, a finger—relative to a camera. The algorithm takes as input a set of 'n' 2D points in the image plane, which correspond to 'n' 3D points in the world coordinate system. The goal is to find the orientation and translation matrices that describe the pose of the 3D points relative to the camera.

Our research focuses on the pose estimation of the index and thumb finger's tip using an algorithm system that integrates MediaPipe's hand detection with the Perspective-n-Point (PnP) algorithm. The system is not designed for capturing video frames but utilizes Mediapipe to identify specific landmarks on the index finger. For example, in the index finger, we use the tip and first knuckle keypoints from Mediapipe, as well as the center point between these two keypoints, to create the n points for index finger. These landmarks are then used as input to the PnP algorithm, which estimates the 3D coordinates of the index finger's tip. The estimated coordinates are subsequently used for kinematic parameter calculation. This approach offers a robust and accurate method for 3D pose estimation of the index finger, providing valuable data for further research and clinical applications.

In this endeavor, we collaborated with physical therapists to create a straightforward motion tracking system aimed at capturing upper extremity functions. The system was designed to analyze the RTG movement using a single smartphone camera. The goal of this study was to compare the parameters derived from our proposed system with those from the EM system. Ultimately, our cost-effective and portable system may offer valuable insights for physical therapists to evaluate their clients' movement in a clinical setting.

1.2 Objective

1) To develop and implement a markerless motion tracking system for the Reach-to-Grasp (RTG) movement using a single smartphone camera. The system should be easy to set up and useful for telemedicine applications. This will be achieved using the MediaPipe framework for hand detection and the Perspective-n-Point (PnP) algorithm for pose estimation.

2) To evaluate the performance and accuracy of the single smartphone camera system by comparing its kinematic parameters with those obtained from a standard motion capture system, specifically the Electromagnetic Motion (EM) tracking system. This comparison will help determine the viability of the smartphone-based system as a cost-effective and portable alternative.

1.3 Hypothesis

1) A single smartphone camera that uses MediaPipe and the PnP algorithm can be effectively used to develop a motion tracking system for the Reach-to-Grasp movement. This system will be capable of providing reliable and accurate 3D pose estimations.

2) The results from the single smartphone camera system will be able to compute kinematic parameters, such as aperture and transport velocity, that are comparable to those obtained from a standard motion capture system like the Electromagnetic Motion (EM) tracking system. This suggests that the smartphone-

based system can serve as a practical and accessible tool for telemedicine applications.

1.4 Scope and limitation of study

1) The study is focused on the development and implementation of a motion tracking system using a single smartphone camera. It investigates the potential of this technology in capturing and analyzing the Reach-to-Grasp (RTG) movement, highlighting its ease of setup and portability, making it suitable for telemedicine applications.

2) The research specifically targets the analysis of the Reach-to-Grasp movement in humans. The key kinematic parameters examined in this study are aperture (the distance between the index finger and thumb during the grasp phase) and transport velocity (the speed at which the hand moves towards the object).

3) The study also involves a detailed comparison of the results obtained from the developed smartphone-based system with those from a higher accuracy Electromagnetic Motion (EM) tracking system. This comparison aims to evaluate the performance and accuracy of the smartphone-based system in measuring the specified kinematic parameters.

4) The detection and tracking accuracy of the system are dependent on the performance of the MediaPipe framework. Any limitations or inaccuracies inherent in MediaPipe's hand detection and pose estimation capabilities will directly impact the overall effectiveness of the motion tracking system developed in this study.

CHAPTER 2

THEORY

2.1 Camera calibration

Camera calibration is a fundamental process in the field of 3D computer vision that aims to establish a precise mathematical relationship between the 3D world and its 2D projection onto the image plane of a camera. This relationship is crucial for accurately extracting metric information from 2D images and performing tasks such as 3D reconstruction, object localization, and camera pose estimation.

The camera calibration process involves determining two sets of parameters: intrinsic parameters and extrinsic parameters. Intrinsic parameters characterize the internal geometry and optical properties of the camera, while extrinsic parameters define the position and orientation of the camera with respect to a known world coordinate system.

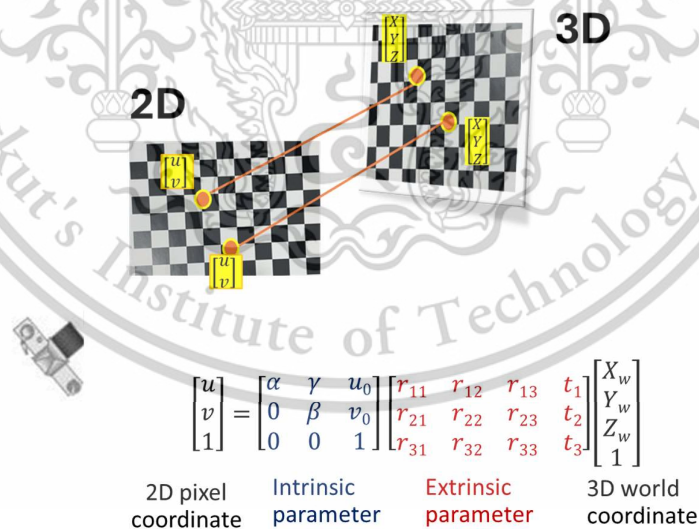


Figure 1 2D to 3D chessboard

The intrinsic parameters of a camera include:

1. Focal Length (f_x, f_y): The distance between the camera's optical center and the image plane, measured in pixels. In an ideal pinhole camera model, f_x and f_y are equal, but they may differ due to non-square pixels.
2. Principal Point (c_x, c_y): The coordinates of the point where the optical axis intersects the image plane. It is usually close to the image center.
3. Skew Coefficient (s): The parameter that represents the skew of the pixel axes. In most modern cameras, the skew is close to zero.

These intrinsic parameters are encapsulated in the camera intrinsic matrix K :

$$K = \begin{bmatrix} f_x & s & c_x \\ 0 & f_y & c_y \\ 0 & 0 & 1 \end{bmatrix}$$

The extrinsic parameters of a camera include

The extrinsic parameters consist of a rotation matrix R and a translation vector t , which define the transformation from the world coordinate system to the camera coordinate system. The rotation matrix R is a 3x3 orthogonal matrix, and the translation vector t is a 3x1 vector. The relationship between a 3D point P_w in the world coordinate system and its corresponding 2D projection p on the image plane can be expressed using the perspective projection equation:

$$p = K[R|t]P_w$$

where $[R|t]$ represents the concatenation of the rotation matrix and the translation vector.

Calibration Techniques

There are various techniques for camera calibration, including:

This material is reserved for educational use only, not allowed for commercial use.

Forbidden to modify the content, and cite the document when use.

1. Direct Linear Transformation (DLT): This method uses a set of known 3D points and their corresponding 2D projections to estimate the camera matrix $P=K[R|t]$ by solving a system of linear equations.

2. Tsai's Method: This two-stage technique first estimates the extrinsic parameters using a set of 3D-2D point correspondences and then solves for the intrinsic parameters.

3. Zhang's Method: This flexible approach uses multiple views of a planar pattern (e.g., a checkerboard) to estimate both intrinsic and extrinsic parameters. It is widely used in computer vision libraries like OpenCV.

Lens Distortion

In addition to the pinhole camera model, real cameras exhibit lens distortions that affect the mapping between 3D points and their 2D projections. The two main types of distortions are:

1.Radial Distortion: Caused by the curvature of the lens, resulting in the "barrel" or "pincushion" effect. It is modeled using the following equations:

$$x_{distorted} = x(1 + k_1r^2 + k_2r^4 + k_3r^6)$$

$$y_{distorted} = y(1 + k_1r^2 + k_2r^4 + k_3r^6)$$

where (x,y) are the undistorted coordinates, $(x_{distorted},y_{distorted})$ are the distorted coordinates, r is the radial distance from the principal point, and k_1, k_2, k_3 are the radial distortion coefficients.

2.Tangential Distortion: Caused by the misalignment of the lens and the image plane. It is modeled using the following equations:

$$x_{distorted} = x + [2p_1xy + p_2(r^2 + 2x^2)]$$

$$y_{distorted} = y + [p_1(r^2 + 2y^2) + 2p_2xy]$$

This material is reserved for educational use only, not allowed for commercial use.

Forbidden to modify the content, and cite the document when use.

where p_1 and p_2 are the tangential distortion coefficients.

The distortion coefficients are estimated during the calibration process and used to undistort the images before further processing.

Zhang's method is a popular camera calibration method that uses a planar checkerboard pattern (chessboard). The process involves taking several images of this pattern at different orientations and then solving for the camera parameters.

overview of the process:

1. Preparation: Print a chessboard pattern and attach it to a flat surface. Ensure the camera and chessboard are in focus and well lit.

2. Capture Images: Take multiple images of the chessboard pattern from different angles and distances. Make sure to cover as much of the field of view as possible.

3. Identify Corners: For each image, identify the intersection points (corners) of the chessboard. This can be done manually, but there are also many computer vision libraries (like OpenCV) that can do this automatically.

4. Estimate Homography: For each image, estimate the homography that maps the 2D chessboard coordinates to the 2D image coordinates. The homography is a 3x3 matrix that encapsulates the rotation and translation between the chessboard and the camera.

5. Compute Camera Parameters: Using the homographies from step 4, compute the camera's intrinsic and extrinsic parameters. The intrinsic parameters include the focal length and optical centers, and the extrinsic parameters describe the camera's orientation and position in space.

1. Projection from world coordinates to image coordinates with camera intrinsics and extrinsics:

$$\begin{bmatrix} u \\ v \\ 1 \end{bmatrix} = \begin{bmatrix} \alpha & \gamma & u_0 \\ 0 & \beta & v_0 \\ 0 & 0 & 1 \end{bmatrix} \begin{bmatrix} r_{11} & r_{12} & r_{13} & t_1 \\ r_{21} & r_{22} & r_{23} & t_2 \\ r_{31} & r_{32} & r_{33} & t_3 \end{bmatrix} \begin{bmatrix} X_w \\ Y_w \\ 0 \\ 1 \end{bmatrix}$$

2. Simplified form when $Z_w=0$ with the same numerical values:

$$\begin{bmatrix} u \\ v \\ 1 \end{bmatrix} = \begin{bmatrix} \alpha & \gamma & u_0 \\ 0 & \beta & v_0 \\ 0 & 0 & 1 \end{bmatrix} \begin{bmatrix} r_{11} & r_{12} & t_1 \\ r_{21} & r_{22} & t_2 \\ r_{31} & r_{32} & t_3 \end{bmatrix} \begin{bmatrix} X_w \\ Y_w \\ 1 \end{bmatrix}$$

3. Numerical example of a Homography matrix H :

$$\begin{bmatrix} u \\ v \\ 1 \end{bmatrix} = H \begin{bmatrix} X_w \\ Y_w \\ 1 \end{bmatrix} = \begin{bmatrix} h_{11} & h_{12} & h_{13} \\ h_{21} & h_{22} & h_{23} \\ h_{31} & h_{32} & h_{33} \end{bmatrix} \begin{bmatrix} X_w \\ Y_w \\ 1 \end{bmatrix}$$

4. Homography vectorization:

$$\begin{bmatrix} u \\ v \\ 1 \end{bmatrix} = \begin{bmatrix} h_1^T \\ h_2^T \\ h_3^T \end{bmatrix} \begin{bmatrix} X_w \\ Y_w \\ 1 \end{bmatrix}$$

Where h_i^T represents the transpose of the i -th row of H , and \mathbf{P} collects the elements of h_1 , h_2 , and h_3 within a parameter vector for optimization or other computational purposes.

5. Equations for computing \mathbf{u} and \mathbf{v} using homography components

$$\mathbf{u} = \frac{\mathbf{h}_1^T \cdot \mathbf{P}}{\mathbf{h}_3^T \cdot \mathbf{P}}, \quad \mathbf{v} = \frac{\mathbf{h}_2^T \cdot \mathbf{P}}{\mathbf{h}_3^T \cdot \mathbf{P}}$$

Where \mathbf{h}_i^T denotes the transpose of the i -th row of the homography matrix \mathbf{H} , and \mathbf{P} is the point in homogenous coordinates.

6. Re-arranged equations to express in terms of zero:

$$(\mathbf{h}_1^T - \mathbf{u} \cdot \mathbf{h}_3^T) \cdot \mathbf{P}_i = 0, \quad (\mathbf{h}_2^T - \mathbf{v} \cdot \mathbf{h}_3^T) \cdot \mathbf{P}_i = 0$$

7. Matrix form of the system for all points:

$$\begin{bmatrix} P_1^T & 0 & -u_1 P_1^T \\ 0 & P_1^T & -v_1 P_1^T \\ \vdots & \vdots & \vdots \\ P_n^T & 0 & -u_n P_n^T \\ 0 & P_n^T & -v_n P_n^T \end{bmatrix} \begin{bmatrix} h_1 \\ h_2 \\ h_3 \end{bmatrix} = \begin{bmatrix} 0 \\ 0 \\ \vdots \\ 0 \\ 0 \end{bmatrix}$$

8. This large matrix equation is typically represented as $\mathbf{A} \cdot \mathbf{H} = 0$, where \mathbf{A} is the coefficient matrix constructed from the point correspondences, and \mathbf{H} represents the flattened homography matrix.

9. Homography Decomposition:

$$\mathbf{H} = (\mathbf{h}_0 \quad \mathbf{h}_1 \quad \mathbf{h}_2) = \mathbf{A} \cdot (\mathbf{r}_0 \quad \mathbf{r}_1 \quad t)$$

$$\mathbf{h}_0^T \cdot (\mathbf{A}^{-1})^T = \mathbf{r}_0^T, \quad \mathbf{h}_1^T \cdot (\mathbf{A}^{-1})^T = \mathbf{r}_1^T$$

As $\mathbf{r}_0, \mathbf{r}_1$ form an orthonormal basis

$$\begin{aligned} \mathbf{r}_0^T \cdot \mathbf{r}_1 &= \mathbf{r}_1^T \cdot \mathbf{r}_0 = 0 & \boxed{1} & \quad \mathbf{r}_0^T \cdot \mathbf{r}_0 = \mathbf{r}_1^T \cdot \mathbf{r}_1 = 1 & \boxed{2} \\ \mathbf{h}_0^T \cdot (\mathbf{A}^{-1})^T \cdot \mathbf{A}^{-1} \cdot \mathbf{h}_1 &= 0 & & \quad \mathbf{h}_0^T \cdot (\mathbf{A}^{-1})^T \cdot \mathbf{A}^{-1} \cdot \mathbf{h}_0 = \mathbf{h}_1^T \cdot (\mathbf{A}^{-1})^T \cdot \mathbf{A}^{-1} \cdot \mathbf{h}_1 & \end{aligned}$$

Zhang substitutes the above expression by a new matrix is \mathbf{B}

$$\mathbf{B} = \mathbf{A}^{-T} \mathbf{A}^{-1} \equiv \begin{bmatrix} B_{11} & B_{12} & B_{13} \\ B_{12} & B_{22} & B_{23} \\ B_{13} & B_{23} & B_{33} \end{bmatrix} \quad \text{assign } \mathbf{b} = [B_{11}, B_{12}, B_{22}, B_{13}, B_{23}, B_{33}]$$

\mathbf{B} is symmetry matrix

$$h_0^T \cdot \mathbf{B} \cdot h_1 = 0 \quad \boxed{1} \quad h_0^T \cdot \mathbf{B} \cdot h_0 - h_1^T \cdot \mathbf{B} \cdot h_1 = 0 \quad \boxed{2}$$

See pattern in constant

$$\begin{aligned} h_0^T \cdot \mathbf{B} \cdot h_1 &= 0 \\ h_0^T \cdot \mathbf{B} \cdot h_0 - h_1^T \cdot \mathbf{B} \cdot h_1 &= 0 \end{aligned} \quad \begin{array}{l} \mathbf{h}_i^T \mathbf{B} \mathbf{h}_j = \mathbf{v}_{ij}^T \mathbf{b} \\ \longrightarrow \end{array} \quad \begin{array}{l} \mathbf{v}_{01}^T \mathbf{b} = 0 \\ (\mathbf{v}_{00} - \mathbf{v}_{11})^T \mathbf{b} = 0 \end{array}$$

Two constraints, from homography, become

$$\begin{array}{l} \mathbf{v}_{01}^T \mathbf{b} = 0 \\ (\mathbf{v}_{00} - \mathbf{v}_{11})^T \mathbf{b} = 0 \end{array} \quad \longrightarrow \quad \begin{bmatrix} \mathbf{v}_{01}^T \\ (\mathbf{v}_{00} - \mathbf{v}_{11})^T \end{bmatrix} \mathbf{b} = 0$$

If observed $n \geq 3$ images of model plane

$$\begin{array}{l} \text{image 1} \text{ ---} \\ \text{image n} \text{ ---} \end{array} \begin{bmatrix} \mathbf{v}_{01}^T \\ (\mathbf{v}_{00} - \mathbf{v}_{11})^T \\ \vdots \\ \mathbf{v}_{01}^T \\ (\mathbf{v}'_{00} - \mathbf{v}'_{11})^T \end{bmatrix} \mathbf{b} = 0$$

$$\mathbf{V} \mathbf{b} = 0$$

estimate \mathbf{b} with SVD

Equation for vector \mathbf{b} representing the elements of matrix \mathbf{B}

$$\mathbf{b} = [B_{11} \quad B_{12} \quad B_{22} \quad B_{13} \quad B_{23} \quad B_{33}]$$

This material is reserved for educational use only, not allowed for commercial use.

Forbidden to modify the content, and cite the document when use.

Relationship between matrix \mathbf{B} and intrinsic camera parameters

We can calculate intrinsic parameter from

$$\mathbf{B} = \mathbf{A}^{-T} \mathbf{A}^{-1}$$

$$\begin{bmatrix} B_{11} & B_{12} & B_{13} \\ B_{12} & B_{22} & B_{23} \\ B_{13} & B_{23} & B_{33} \end{bmatrix} = \begin{bmatrix} \frac{1}{\alpha^2} & -\frac{\gamma}{\alpha^2\beta} & \frac{v_0\gamma - u_0\beta}{\alpha^2\beta} \\ -\frac{\gamma}{\alpha^2\beta} & \frac{\gamma^2}{\alpha^2\beta^2} + \frac{1}{\beta^2} & -\frac{\gamma(v_0\gamma - u_0\beta)}{\alpha^2\beta^2} + \frac{v_0}{\beta^2} \\ \frac{v_0\gamma - u_0\beta}{\alpha^2\beta} & -\frac{\gamma(v_0\gamma - u_0\beta)}{\alpha^2\beta^2} + \frac{v_0}{\beta^2} & \frac{(v_0\gamma - u_0\beta)^2}{\alpha^2\beta^2} + \frac{v_0^2 + 1}{\beta^2} \end{bmatrix}$$

This matrix \mathbf{B} is a representation of the intrinsic parameters of the camera, where:

α is the focal length in terms of pixels in the x-direction

β is the focal length in terms of pixels in the y-direction

γ is the skew coefficient between x and y coordinates

u_0 and v_0 are the coordinates of the principal point of the camera.

Calculation Steps for get intrinsic. Define variables w , d , α , β , γ , u_c , and v_c based on elements of \mathbf{B}

$$w \leftarrow B_0 B_2 B_5 - B_1^2 B_5 - B_0 B_4^2 + 2 B_1 B_3 B_4 - B_2 B_3^2$$

$$d \leftarrow B_0 B_2 - B_1^2$$

$$\alpha \leftarrow \sqrt{\frac{w}{d \cdot B_0}}$$

$$\beta \leftarrow \sqrt{\frac{w}{d^2 \cdot B_0}}$$

$$\gamma \leftarrow \frac{w}{d^2 \cdot B_0} \cdot B_1$$

$$u_c \leftarrow \frac{B_1 B_4 - B_2 B_3}{d}$$

$$v_c \leftarrow \frac{B_1 B_3 - B_0 B_4}{d}$$

Assemble the Intrinsic Matrix

$$A \leftarrow \begin{bmatrix} \alpha & \gamma & u_c \\ 0 & \beta & v_c \\ 0 & 0 & 1 \end{bmatrix}$$

This sequence of equations effectively extracts the intrinsic camera parameters—focal lengths (α and β), skew (γ), and principal point coordinates (u_c and v_c)—from the matrix B .

Calculating Extrinsic parameter from Homography and Intrinsic parameter

$$\begin{bmatrix} u \\ v \\ 1 \end{bmatrix} = \begin{bmatrix} \alpha & \gamma & u_0 \\ 0 & \beta & v_0 \\ 0 & 0 & 1 \end{bmatrix} \begin{bmatrix} r_{11} & r_{12} & r_{13} & t_1 \\ r_{21} & r_{22} & r_{23} & t_2 \\ r_{31} & r_{32} & r_{33} & t_3 \end{bmatrix} \begin{bmatrix} X_w \\ Y_w \\ Z_w \\ 1 \end{bmatrix}$$

2D pixel coordinate
Intrinsic parameter
Extrinsic parameter
3D world coordinate

Decomposition of the Homography Matrix:

Given a homography matrix H and intrinsic parameters matrix A , the extrinsic parameters can be calculated as follows:

$$H = [h_1 \quad h_2 \quad h_3] = A[r_1 \quad r_2 \quad t]$$

Calculate Rotation Vectors:

The columns r_1 and r_2 are computed by inverting A and multiplying it with h_1 and h_2 respectively:

$$r_1 = A^{-1}h_1, \quad r_2 = A^{-1}h_2$$

\mathbf{r}_3 , the third column of the rotation matrix, is calculated as the cross product of \mathbf{r}_1 and \mathbf{r}_2 :

$$\mathbf{r}_3 = \mathbf{r}_1 \times \mathbf{r}_2$$

Calculate Translation Vector:

The translation vector \mathbf{t} is calculated by multiplying the inverse of \mathbf{A} with \mathbf{h}_3 :

$$\mathbf{t} = \mathbf{A}^{-1}\mathbf{h}_3$$



Figure 2 chessboard multiple view

2.2 Motion Capture Systems

Motion Capture (MoCap) Systems are technologies designed to monitor and track the movement of objects. These systems can be developed using a variety of technologies, and they are primarily categorized into two types: optical-based and non-optical based systems.

1) Non-optical based MoCap Systems: These systems do not rely on cameras or light to capture motion. Instead, they use other types of detectors to track movement. Examples of non-optical systems include those that use Inertial Measurement Units (IMUs), which capture motion through accelerometers and gyroscopes, and electromagnetic sensors, which track the movement of objects within a magnetic field. This study using electromagnetic for standard

2) Optical-based MoCap Systems: These systems utilize image sensors, such as video cameras, to capture motion. They work by tracking markers or features, which can either be placed on the object (marker-based) or identified through image analysis (markerless). The captured data is then processed to construct a digital representation of the object's movement.

Each type of system has its own advantages and limitations, and the choice between optical and non-optical systems often depends on the specific requirements of the application.

2.3 MediaPipe Hands

MediaPipe Hands, developed by Google, is a specialized machine learning framework for hand tracking and pose estimation. The framework operates through a two-step process for enhanced accuracy and robustness. In Step 1, a palm detection model is employed to scan the input frame and identify the bounding box around the hand or hands present. This model is trained to recognize the unique features and contours of a palm, effectively isolating the hand region from the rest of the image. Once the palm area is detected, Step 2 is initiated. Here, a hand landmark model takes over, focusing on the previously identified bounding box. This model is designed to estimate 21 3D keypoints, which represent anatomical landmarks on the hand, such as the tips and bases of each finger, the palm, and the wrist. These keypoints are then output as 3D coordinates, providing a detailed representation of hand pose. The framework is versatile, capable of handling both single and multiple hands within the same frame, and finds extensive applications in fields like augmented reality, sign language recognition, and human-computer interaction.

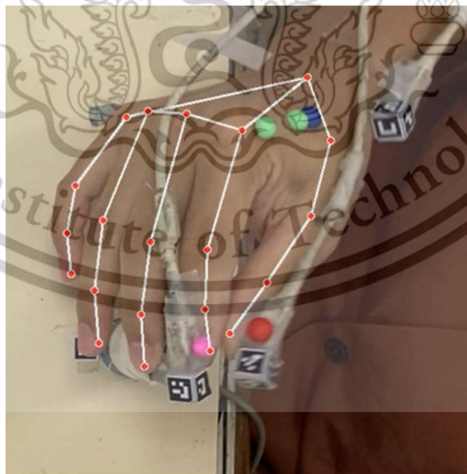


Figure 3 Pose estimation by Mediapipe

2.3.1 Architecture

Hand tracking system employs a machine learning (ML) pipeline that integrates two distinct models to enhance tracking accuracy and efficiency:

1. Palm Detector Model: This model processes the entire input image to detect the presence and location of palms. It outputs an oriented hand bounding box

2. Hand Landmark Model: Upon receiving the cropped image of the hand from the palm detector, this model predicts high-fidelity 2.5D hand landmarks.

The integration of these models reduces the necessity for extensive data augmentation techniques such as rotations, translations, and scaling. This is because the hand landmark model receives a well-oriented and scaled input, allowing it to focus primarily on the accuracy of landmark localization. In real-time scenarios, the system optimizes processing by reusing the landmark predictions from the previous frame to define the bounding box for the current frame:

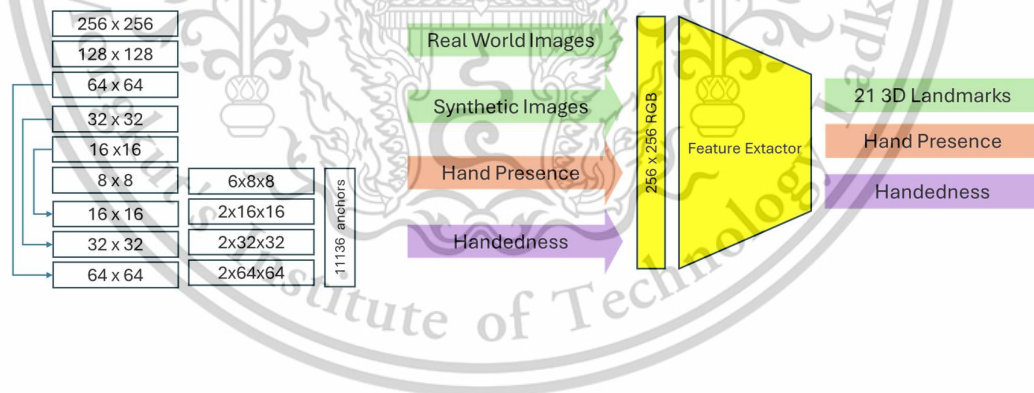


Figure 4 Palm detector model architecture(left). Hand landmark model architecture (right) .

The model has three outputs sharing a feature extractor. Each head is trained by correspondent datasets marked in the same color.

The BlazePalm Detector employs a single-shot detection model, optimized for mobile real-time applications, to identify initial hand locations. This model, inspired by BlazeFace, is designed to tackle the inherent complexities of hand detection, including the wide range of hand sizes, occlusion challenges, and the absence of high-contrast features typical of faces. The approach can be broken down into several key strategies, each contributing to the model's effectiveness:

1. Palm Detection Strategy:

The model focuses on detecting palms rather than the entire hand, simplifying the problem to identifying more rigid objects. This is represented as:

$$\mathbf{B}_{\text{palm}} = \text{Detect}(\mathbf{I})$$

where \mathbf{B}_{palm} denotes the bounding box of the detected palm and \mathbf{I} represents the input image. Palms are detected using square bounding boxes, reducing the complexity and number of anchors needed.

2. Feature Extraction:

An encoder-decoder architecture, akin to a Feature Pyramid Network (FPN), is utilized for feature extraction. This allows for enhanced scene context awareness, crucial for detecting smaller objects like palms within a wide range of scales. The feature extraction process can be mathematically described as:

$$\mathbf{F} = \text{ExtractFeatures}(\mathbf{I})$$

where \mathbf{F} represents the extracted features from the input image \mathbf{I} .

3. Focal Loss Minimization:

To address the challenge of a large number of anchors due to high scale variance, the focal loss is minimized during training. This is crucial for focusing the model's learning on hard-to-detect examples and is represented as:

$$L_{\text{focal}} = -\alpha_t(1-p_t)^\gamma \log(p_t)$$

where L_{focal} is the focal loss, α_t is the alpha factor, p_t is the predicted probability of the target class, and γ is the focusing parameter.

The Hand Landmark Model operates subsequent to the palm detection phase, focusing on precise localization of hand landmarks within the detected regions. This model is designed to output 21 2.5D coordinates representing hand landmarks, along with additional classifications regarding hand presence and handedness. The mathematical representation of the model's operations can be detailed as follows:

1. Landmark Localization:

The model regresses to 21 hand landmarks, each consisting of \mathbf{x} , \mathbf{y} , and relative depth coordinates. This can be represented by:

$$\{\mathbf{L}_i\}_{i=1}^{21} = \text{Localize}(\mathbf{I}_{\text{cropped}})$$

where $\{\mathbf{L}_i\}$ denotes the set of 21 landmarks and $\mathbf{I}_{\text{cropped}}$ is the cropped image of the hand region provided by the palm detector.

2. Hand Presence Flag:

A probability score indicating the presence of a hand in the input image is computed, which can be represented as:

$$\mathbf{P}_{\text{hand}} = \text{Probability}(\mathbf{I}_{\text{cropped}})$$

where \mathbf{P}_{hand} is the probability of hand presence.

3. Handedness Classification:

The model classifies whether the detected hand is left or right, which is crucial for applications requiring differentiated functionalities for each hand. This is represented as:

$$\mathbf{H} = \text{ClassifyHandedness}(\mathbf{I}_{\text{cropped}})$$

where \mathbf{H} indicates the handedness (left or right).

The model's training incorporates both real-world and synthetic datasets to learn the 2D coordinates, while the relative depth is specifically learned from synthetic images. This dual-source training enhances the model's robustness to variations in hand visibility and occlusion. Additionally, to ensure reliability in real-time applications, the model includes a mechanism to trigger a reset in tracking if the hand presence probability falls below a certain threshold. This is crucial for

maintaining continuous and accurate tracking, especially in dynamic environments. The model's architecture is optimized for real-time inference on mobile GPUs, with variations designed to accommodate different computational resources, such as CPUs on mobile devices and more powerful desktop setups.

The dataset and annotation process for the hand tracking system is structured to address various aspects of hand detection and landmark localization through a combination of real-world, in-house, and synthetic datasets:

1. In-the-Wild Dataset: This dataset comprises 6,000 images featuring a broad range of conditions such as geographical diversity, different lighting scenarios, and varied hand appearances. However, it lacks images with complex hand articulations. This dataset primarily supports the palm detector, focusing on hand localization across diverse appearances.

2. In-House Collected Gesture Dataset: Containing 10,000 images, this dataset is designed to cover various angles of all physically possible hand gestures, captured from 30 individuals. The backgrounds in these images are relatively uniform, limiting variability. This dataset complements the in-the-wild dataset by enhancing the robustness of the hand landmark model against different gesture types.

3. Synthetic Dataset: To address gaps in hand pose coverage and depth perception, a synthetic dataset is created using a commercial 3D hand model rigged with 24 bones and 36 blendshapes for detailed finger and palm movements. This model is rendered over various backgrounds, producing 100,000 images from video sequences of transitioning hand poses. Each pose is rendered with random high-dynamic-range lighting and from three different camera angles. This dataset is crucial for training the hand landmark model, especially for depth learning and complex pose recognition.

Annotation Process:

- Real-world images are annotated with 21 hand landmarks. For synthetic images, projected ground-truth 3D joints are used for annotation.
- A subset of real-world images is selected as positive examples for hand presence, while regions excluding annotated hand areas serve as negative examples.
- Handedness is annotated on a subset of real-world images to provide data necessary for distinguishing between left and right hands.

Each dataset plays a specific role in training the models, with the in-the-wild dataset focusing on palm detection due to its high variability and the other datasets enhancing the hand landmark model's accuracy and robustness.

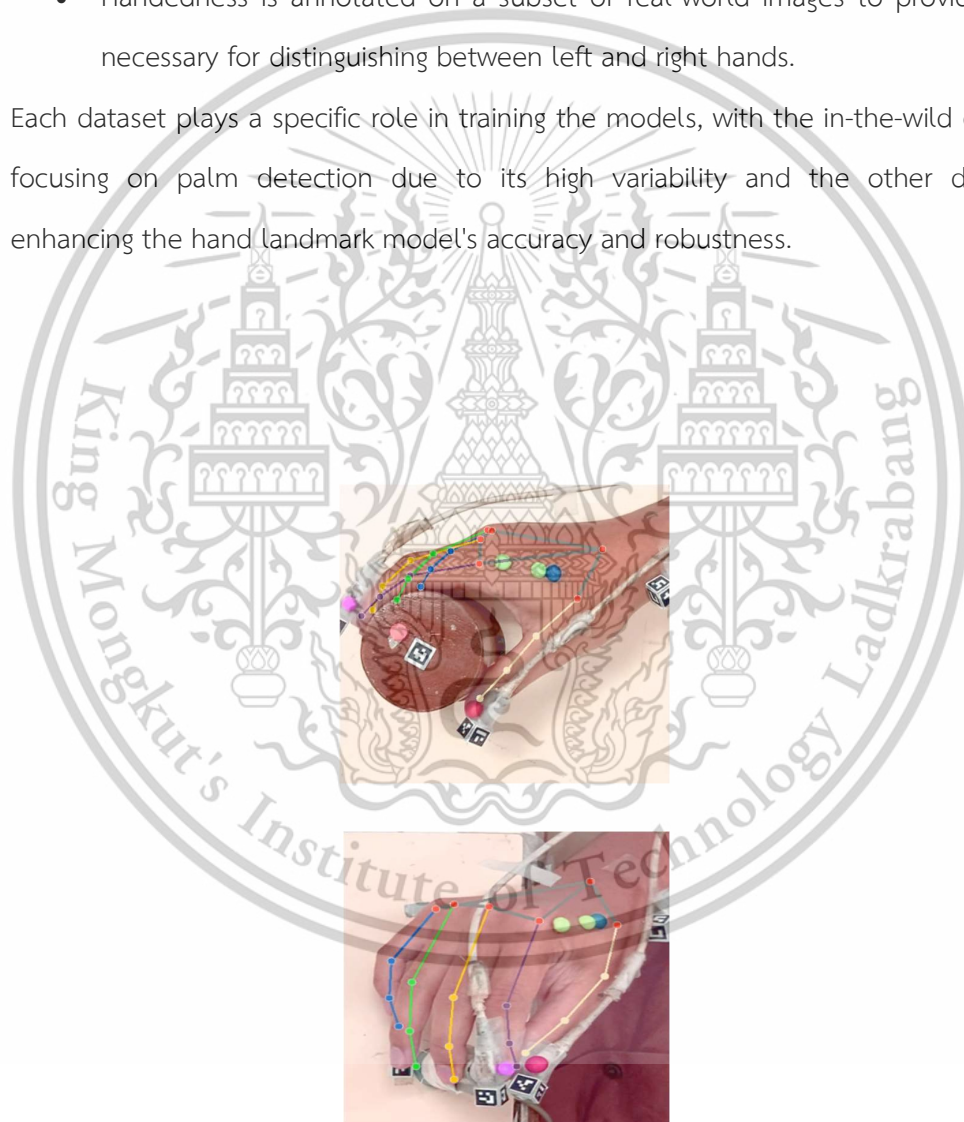


Figure 5 Examples of datasets. (Top): Annotated realworld images. (Bottom): Rendered synthetic hand images with ground truth annotation.

2.3.2 Tracking

After the initial detection of the hand keypoints, the tracking algorithm uses the spatial location of these keypoints from the previous frame to predict their location in the current frame. This prediction serves as a region of interest (ROI) for the palm detection model in the next frame, effectively narrowing down the search area and making the process more efficient. By using the keypoints' spatial information from previous frames, MediaPipe is able to achieve smooth and robust tracking of hand movements across consecutive frames. This tracking algorithm is optimized for real-time performance and is capable of handling rapid hand movements and occlusions.

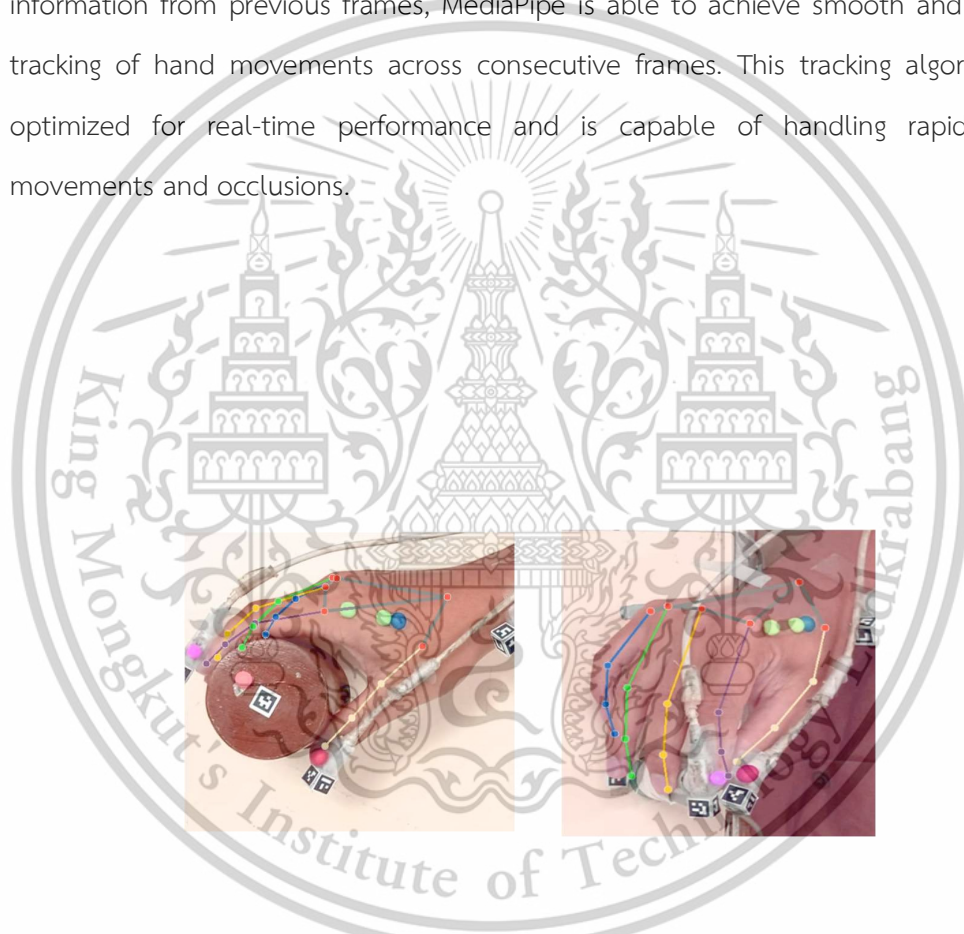


Figure 6 Tracking by Mediapipe

2.4 PnP algorithm

The Perspective-n-Point (PnP) algorithm is a cornerstone technique in computer vision for estimating the pose of a 3D object in a scene relative to a calibrated camera. The term "pose" here refers to the spatial orientation and position of the object, represented by rotation and translation matrices. The "n" in PnP denotes the number of corresponding 2D-3D point pairs used for the estimation. Specifically, the algorithm takes as input a set of 3D points on the object and their corresponding 2D projections in the image. It then computes the rotation and translation that would allow these 3D points to align with the 2D points when projected using the camera's intrinsic parameters

1. Given Data Preparation:

- 3D Points: X_i where $i=1,2,\dots,n$

- $X_1 = \begin{bmatrix} 1 \\ 2 \\ 5 \end{bmatrix}$

- $X_2 = \begin{bmatrix} 2 \\ 3 \\ 6 \end{bmatrix}$

- $X_3 = \begin{bmatrix} 3 \\ 1 \\ 4 \end{bmatrix}$

- 2D Points: x_i where $i=1,2,\dots,n$

- $x_1 = \begin{bmatrix} 320 \\ 240 \end{bmatrix}$

- $x_2 = \begin{bmatrix} 400 \\ 300 \end{bmatrix}$

- $x_3 = \begin{bmatrix} 450 \\ 350 \end{bmatrix}$

These points correspond such that each 3D point X_i is projected onto the 2D point x_i .

2. Camera Intrinsic Matrix (K):

Defined as:

$$\bullet K = \begin{bmatrix} f_x & s & c_x \\ 0 & f_y & c_y \\ 0 & 0 & 1 \end{bmatrix}$$

$$\bullet K = \begin{bmatrix} 1000 & 0 & 300 \\ 0 & 1000 & 200 \\ 0 & 0 & 1 \end{bmatrix}$$

$$\bullet \text{Parameters: } f_x = f_y = 1000, s = 0, c_x = 300, c_y = 200$$

Where f_x, f_y are the focal lengths, s is the skew, and (c_x, c_y) are the coordinates of the optical center.

3. Homogeneous Coordinates Conversion and Camera Matrix Application:

Convert 2D Points into Homogeneous Coordinates:

$$\bullet \mathbf{x}_1^h = \begin{bmatrix} 320 \\ 240 \\ 1 \end{bmatrix}$$

$$\bullet \mathbf{x}_2^h = \begin{bmatrix} 400 \\ 300 \\ 1 \end{bmatrix}$$

$$\bullet \mathbf{x}_3^h = \begin{bmatrix} 450 \\ 350 \\ 1 \end{bmatrix}$$

Apply the Camera Matrix:

$$\mathbf{x}'_1 = K\mathbf{X}_1 = \begin{bmatrix} 1000 & 0 & 300 \\ 0 & 1000 & 200 \\ 0 & 0 & 1 \end{bmatrix} \begin{bmatrix} 1 \\ 2 \\ 5 \end{bmatrix} = \begin{bmatrix} 1300 \\ 2200 \\ 5 \end{bmatrix} \rightarrow \begin{bmatrix} 260 \\ 440 \\ 1 \end{bmatrix}$$

$$\mathbf{x}'_2 = K\mathbf{X}_2 = \begin{bmatrix} 1000 & 0 & 300 \\ 0 & 1000 & 200 \\ 0 & 0 & 1 \end{bmatrix} \begin{bmatrix} 2 \\ 3 \\ 6 \end{bmatrix} = \begin{bmatrix} 2300 \\ 3200 \\ 6 \end{bmatrix} \rightarrow \begin{bmatrix} 383.33 \\ 533.33 \\ 1 \end{bmatrix}$$

$$\mathbf{x}'_3 = K\mathbf{X}_3 = \begin{bmatrix} 1000 & 0 & 300 \\ 0 & 1000 & 200 \\ 0 & 0 & 1 \end{bmatrix} \begin{bmatrix} 3 \\ 1 \\ 4 \end{bmatrix} = \begin{bmatrix} 3300 \\ 1200 \\ 4 \end{bmatrix} \rightarrow \begin{bmatrix} 825 \\ 300 \\ 1 \end{bmatrix}$$

4. Solving for R and t using SVD

- The relationship between the 3D points and their image projections is given by:

$$x_i \sim K[R|t]X_i$$

- Where R is the rotation matrix, t is the translation vector, and \sim denotes equality up to a scale factor.

The equation above can be expanded as:

$$\begin{bmatrix} u_i \\ v_i \\ 1 \end{bmatrix} = K[R|t] \begin{bmatrix} X_i \\ Y_i \\ Z_i \\ 1 \end{bmatrix}$$

$$\begin{bmatrix} 320 \\ 240 \\ 1 \end{bmatrix} = \begin{bmatrix} 1000 & 0 & 300 \\ 0 & 1000 & 200 \\ 0 & 0 & 1 \end{bmatrix} [R|t] \begin{bmatrix} 1 \\ 2 \\ 5 \\ 1 \end{bmatrix}$$

- Here (u_i, v_i) are the pixel coordinates of x_i ,

Solving the System by Direct Linear Transform (DLT): Setup the equation $AX=b$ where A is constructed using the elements from each projection equation and b is the flattened vector of the right-hand sides (the 2D point coordinates after being multiplied by the camera matrix).

$$A = \begin{bmatrix} 1 & 2 & 5 & 1 \\ 2 & 3 & 6 & 1 \\ 3 & 1 & 4 & 1 \end{bmatrix}, \quad b = \begin{bmatrix} 260 \\ 440 \\ 1 \\ 383.33 \\ 533.33 \\ 1 \\ 825 \\ 300 \\ 1 \end{bmatrix}$$

Using SVD to solve the homogeneous system and find the parameters in X

Step 1: $AX = B$

$$\begin{bmatrix} 1 & 2 & 5 & 1 \\ 2 & 3 & 6 & 1 \\ 3 & 1 & 4 & 1 \end{bmatrix} X = \begin{bmatrix} 260 \\ 440 \\ 1 \end{bmatrix}$$

Step 2: $(U\Sigma V^T)X = B$

$$\left(\begin{bmatrix} -0.46 & 0.88 & 0.10 \\ -0.66 & -0.37 & -0.65 \\ -0.60 & -0.30 & 0.74 \end{bmatrix} \begin{bmatrix} 11.04 & 0 & 0 \\ 0 & 2.44 & 0 \\ 0 & 0 & 0.75 \end{bmatrix} \begin{bmatrix} -0.27 & -0.42 & -0.87 & -0.11 \\ 0.74 & -0.67 & 0.05 & -0.05 \\ 0.61 & 0.61 & -0.43 & -0.25 \end{bmatrix} \right) X = \begin{bmatrix} -181.66 \\ -30.83 \\ -153.25 \end{bmatrix}$$

Step 3: Multiply Both Sides by U^T

$$\begin{bmatrix} 11.04 & 0 & 0 \\ 0 & 2.44 & 0 \\ 0 & 0 & 0.75 \end{bmatrix} \begin{bmatrix} -0.27 & -0.42 & -0.87 & -0.11 \\ 0.74 & -0.67 & 0.05 & -0.05 \\ 0.61 & 0.61 & -0.43 & -0.25 \end{bmatrix} X = \begin{bmatrix} -181.66 \\ -30.83 \\ -153.25 \end{bmatrix}$$

Step 4: Let $Y = V^T X$

$$\Sigma Y = \begin{bmatrix} -181.66 \\ -30.83 \\ -153.25 \end{bmatrix}$$

Step 5: Solve for Y

$$Y = \Sigma^+ \begin{bmatrix} -181.66 \\ -30.83 \\ -153.25 \end{bmatrix}$$

$$Y = \begin{bmatrix} 0.0906 & 0 & 0 \\ 0 & 0.4098 & 0 \\ 0 & 0 & 1.3333 \end{bmatrix} \begin{bmatrix} -181.66 \\ -30.83 \\ -153.25 \end{bmatrix} = \begin{bmatrix} -16.47 \\ -12.62 \\ -204.33 \end{bmatrix}$$

Step 6: Solve for X

$$X = VY$$

$$X = \begin{bmatrix} -0.27 & 0.74 & 0.61 \\ -0.42 & -0.67 & 0.61 \\ -0.87 & 0.05 & -0.43 \\ -0.11 & -0.05 & -0.25 \end{bmatrix} \begin{bmatrix} -16.47 \\ -12.62 \\ -204.33 \end{bmatrix} = \begin{bmatrix} 168.75 \\ 98.01 \\ 255.25 \\ 20.57 \end{bmatrix}$$

Assuming X contains parameters representing both rotation and translation, we can decompose it as follows:

$$X = [\text{rotation and translation parameters}]$$

Typical Form of X

For a 3D to 2D projection, the typical form of the extrinsic parameters might be represented as:

$$X = \begin{bmatrix} r_{11} & r_{12} & r_{13} & t_x \\ r_{21} & r_{22} & r_{23} & t_y \\ r_{31} & r_{32} & r_{33} & t_z \end{bmatrix}$$

Where:

- r_{ij} are the elements of the rotation matrix R .
- t_x, t_y, t_z are the elements of the translation vector t .

Steps to Extract R and t

1. Obtain the Rotation Matrix R : Extract the first 3x3 submatrix from X to get R .
2. Obtain the Translation Vector t : Extract the last column of X to get t .

Given the assumed values, the solution vector X can be correctly decomposed into

$$X_{\text{reshaped}} = \begin{bmatrix} 168.75 & 98.01 & 255.25 & 20.57 \\ -45.32 & 73.12 & 120.25 & 18.93 \\ 30.12 & 55.67 & 110.50 & 22.15 \end{bmatrix}$$

- **Rotation Matrix R :**

$$R = \begin{bmatrix} 168.75 & 98.01 & 255.25 \\ -45.32 & 73.12 & 120.25 \\ -30.12 & 55.67 & 110.50 \end{bmatrix}$$

- **Translation Vector t :**

$$t = \begin{bmatrix} 20.57 \\ 18.93 \\ 22.15 \end{bmatrix}$$

the rotation matrix R and the translation vector t as follows:

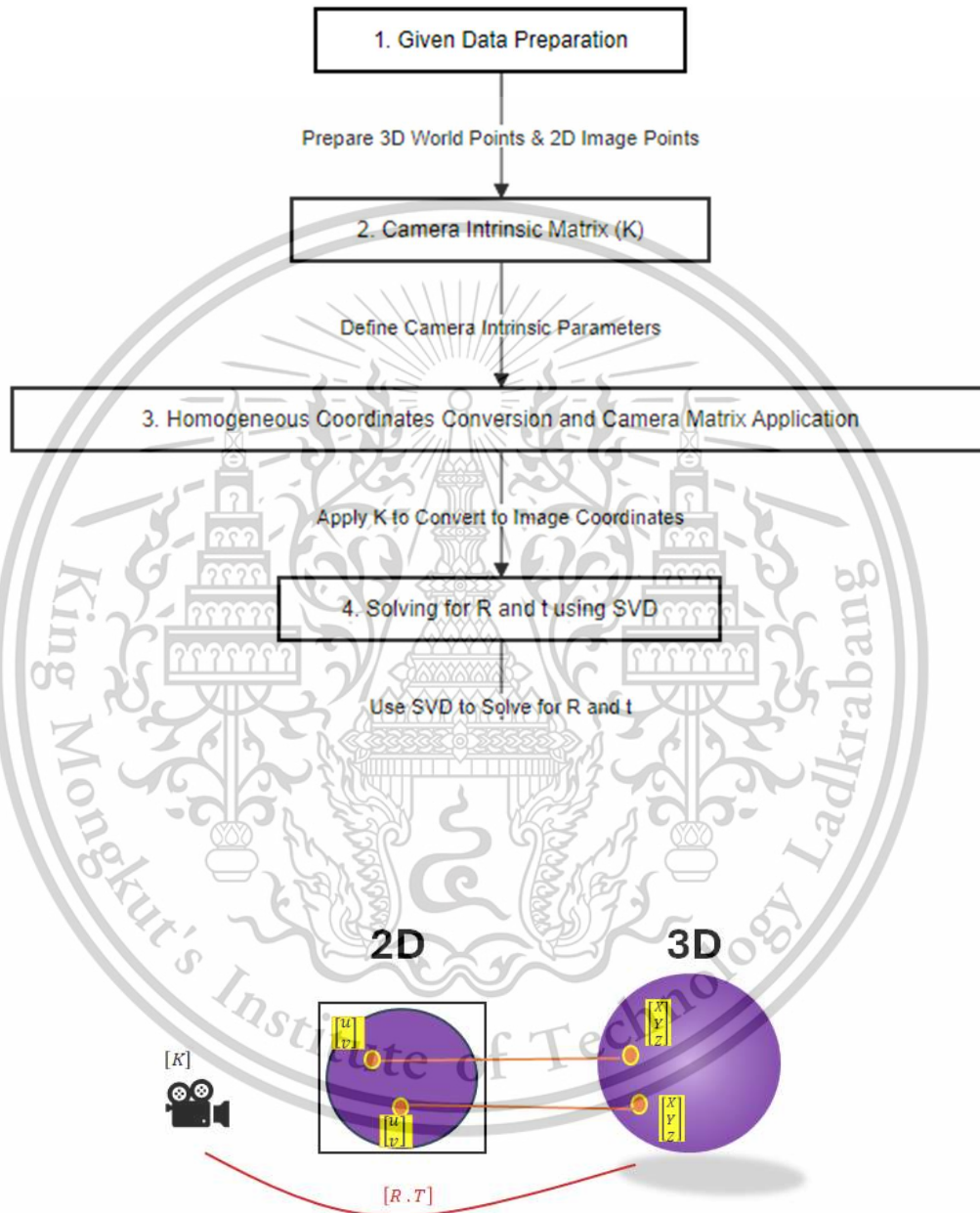


Figure 7 Perspective-n-Point (PnP) algorithm

CHAPTER 3

RESEARCH METHODS

3.1 Camera calibration procedure

Camera calibration using a chessboard pattern is a common method to determine the intrinsic and extrinsic parameters of a camera. This process helps correct lens distortion and improve the accuracy of 3D scene reconstruction. Here's a detailed step-by-step guide on how to perform camera calibration using a chessboard: By following these steps and accurately estimating the necessary parameters, the calibration process can be successfully completed, leading to improved accuracy and reliability in subsequent operations.

Step 1: Prepare the Chessboard

1. **Obtain or create a chessboard pattern.** Use a chessboard with a known number of squares (e.g., 8x8, 9x6). The size of the squares should be measurable, as this is essential for calibration accuracy.
2. **Print the chessboard** on a flat, rigid material to prevent warping during the calibration process.

Step 2: Set Up the Camera

1. **Mount the camera on a stable platform** to minimize movement during the calibration process.
2. **Ensure the entire chessboard is visible** to the camera from various angles and distances.

Step 3: Capture Images

1. **Take multiple photographs of the chessboard** from different angles and distances. Ensure the chessboard fills the frame in some shots and appears in the corners in others to capture a range of distortions.
2. **Capture at least 10-20 images** to cover all parts of the camera's field of view.

Step 4: Image Processing

1. **Convert images to grayscale** to simplify the detection of corners.
2. **Use a corner detection algorithm** like the Harris corner detector or the OpenCV function `findChessboardCorners()` to identify the internal corners of the chessboard in each image.

Step 5: Camera Calibration

1. **Input the detected corners (image points) and the real-world coordinates of the chessboard corners (object points)** into a camera calibration algorithm.
2. **Use OpenCV's `calibrateCamera()` function**, which requires object points, image points, and the shape of the image obtained from the camera. This function returns the camera matrix, distortion coefficients, rotation, and translation vectors.

Step 6: Evaluate the Calibration

1. **Check the re-projection error**, which quantifies the accuracy of the calibration. A lower re-projection error indicates a more accurate calibration.
2. **Visualize the results** by using the distortion coefficients and camera matrix to undistort the images and compare them to the original images.

Step 7: Save the Calibration Parameters

1. **Store the camera matrix and distortion coefficients** for future use

This material is reserved for educational use only, not allowed for commercial use.

Forbidden to modify the content, and cite the document when use.

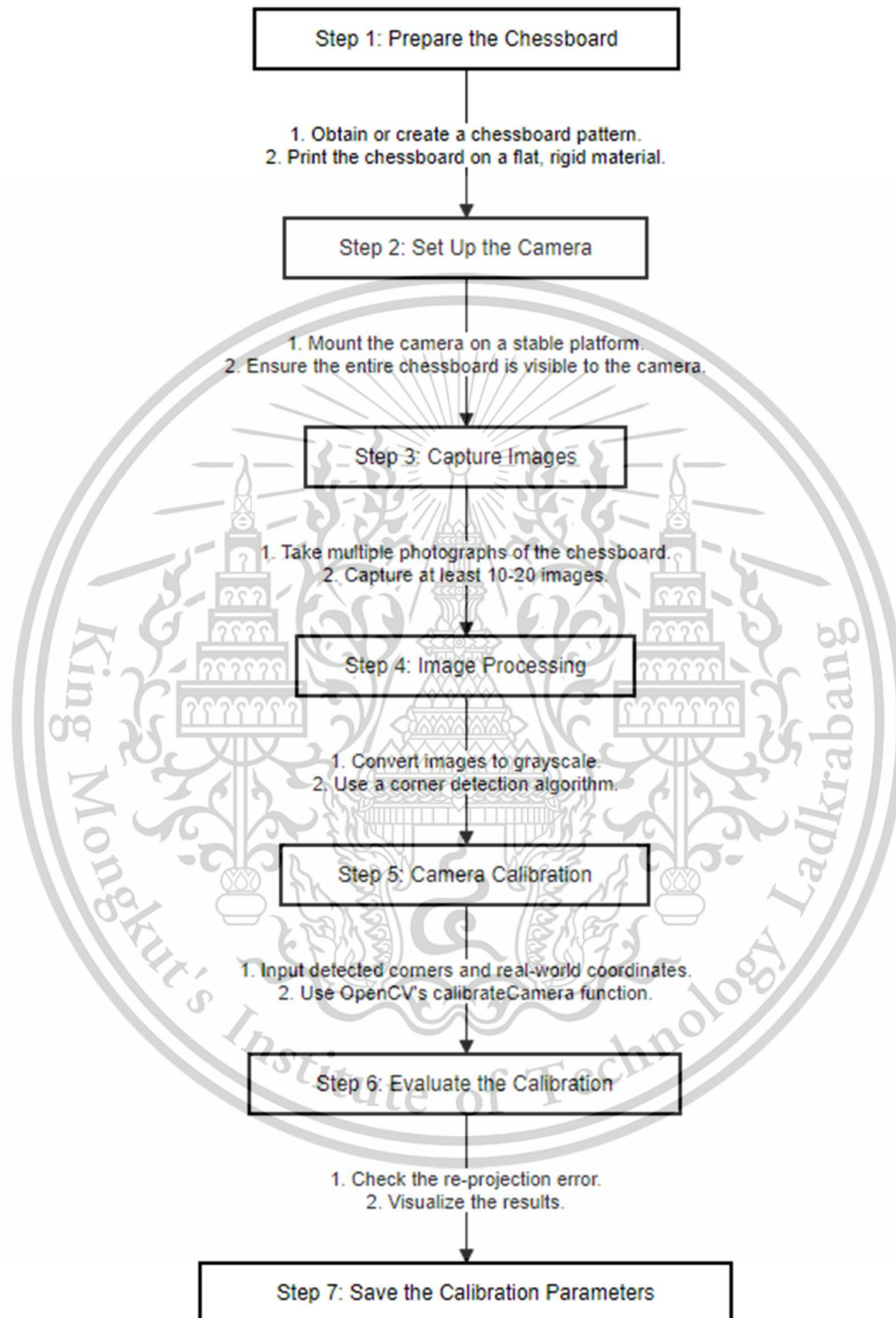


Figure 8 Chessboard for camera calibration

3.2 Preparation for Experiment

As shown in Fig. 7, a participant was asked to sit and place their tested hand on the table at the starting point. The starting point was located 30 centimeters away from the target object, which was a wooden dowel with a diameter of 7.5 centimeters. The participant's hand was equipped with three electromagnetic sensors: two on the tips of the thumb and index fingers, and the third on the radial styloid process. These three sensors were part of the electromagnetic motion tracking system (Motion Monitor, Innsport, Inc, IL, USA [6]). The motion was recorded at a sampling rate of 100 Hz.

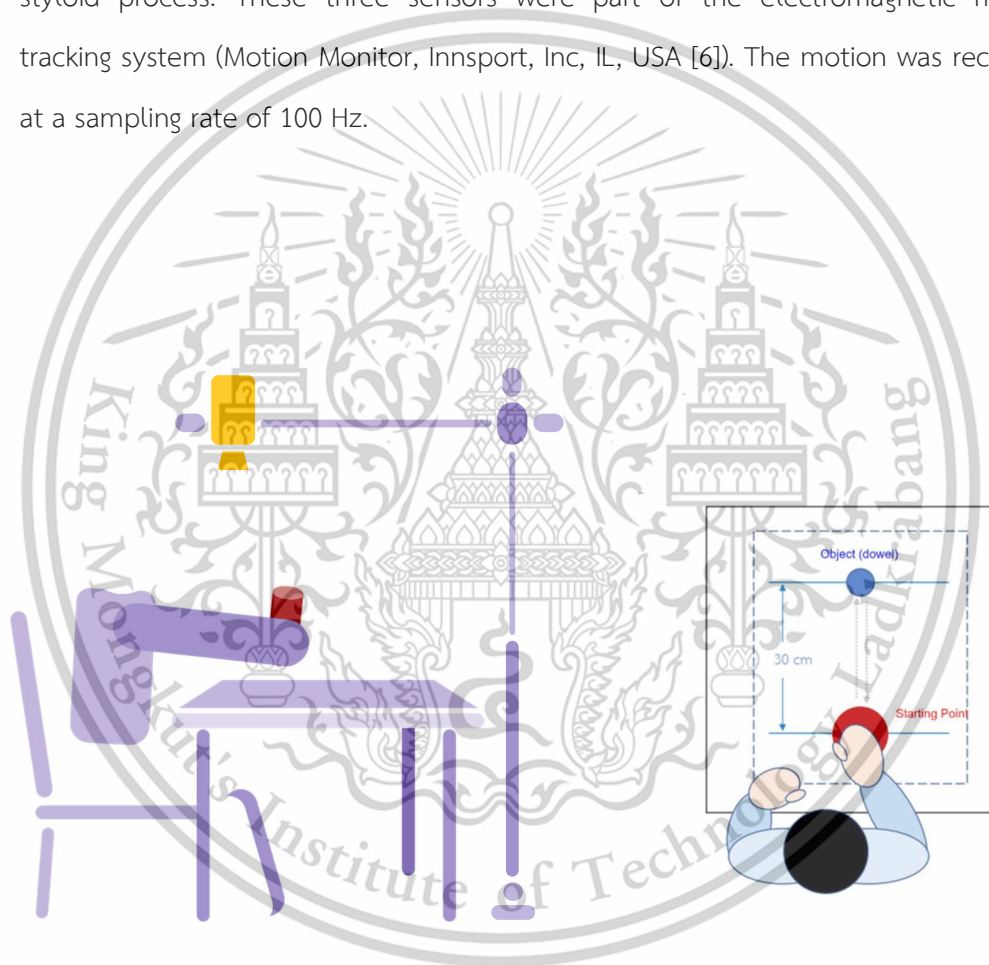


Figure 9 Setup of experiment

The participant's hand was equipped with three electromagnetic sensors: two on the tips of the thumb and index fingers, and the third on the radial styloid process. These three sensors were part of the electromagnetic motion tracking

system (Motion Monitor, Innsport, Inc, IL, USA [6]). The motion was recorded at a sampling rate of 100 Hz.

The participant's hand had four small foam balls of different colors (5-millimeter diameter) attached to it, placed over the latex glove. These balls served as markers for our optical motion capture system, and their positions can be seen in Fig 5. Precisely, the yellow and red balls were positioned at the tips of the thumb and index fingers, respectively. We measured the displacement between these two balls to determine the hand aperture. Additionally, we placed a blue ball on the lateral side of the wrist joint to calculate the hand transport velocity. The two green balls acted as calibrated markers, providing the necessary information to estimate the distance from the camera. Speaking of the camera, was positioned above the table and recorded the movement captured by the optical motion capture system at a rate of 60 frames per second.



Figure 10 The locations of markers for motion capture system

Once the participant heard the "GO" signal, they immediately initiated a sequence of actions, including reaching, grasping, lifting, holding, putting down, releasing the object, and returning their hand to the starting position. This task was repeated for a total of 5 trials. The position data captured by the electromagnetic sensors were then extracted and stored in the computer. Additionally, the video data recorded by the camera underwent an offline conversion process, resulting in a series of static images. The color markers' positions were identified in each of these images and subsequently transformed into 3D coordinates using Python software.

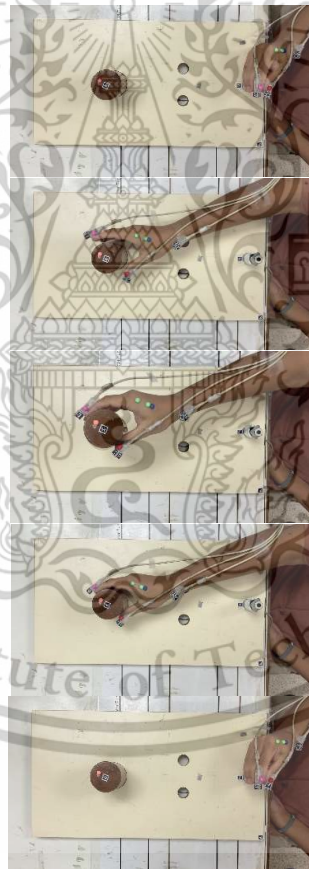


Figure 11 Reach to Grasp motion

3.3 Compute 3D coordinates

This is a step of the program for compute 3D coordinates by Python and Opencv using PnP algorithm and Mediapipe

1. Start: The entry point of the program.
2. Model Points: Initialize a 3D model point matrix to represent the index finger's tip and its thickness.
3. CSV File Setup: Open a new CSV file and write the header for storing the estimated 3D coordinates.
4. Video Capture: Open a video file and prepare to read frames in a loop.
5. While Loop Start: The beginning of the loop that will continuously read video frames and perform hand tracking and 3D pose estimation.
6. Read Frame: Read a single frame from the video file.
7. Hand Tracking: Use MediaPipe to track the hand and get the 2D coordinates of specific landmarks on the index finger.
8. Drawing Landmarks: Utilize MediaPipe's drawing utility to visualize the hand landmarks on the video frame.
9. Intermediate Points: Calculate intermediate 2D points between the detected landmarks to represent the index finger's length and thickness.
10. Pose Estimation: Use the PnP algorithm to estimate the 3D coordinates of the index finger tip based on the 2D image points and 3D model points.
11. CSV Writing: Write the estimated 3D coordinates to the CSV file.
12. Display and Exit: Display the video frame with hand landmarks. The loop breaks if the 'q' key is pressed, leading to file cleanup.
13. File Cleanup: Close the video capture and the CSV file.
14. End: The program terminates.

Each step is crucial for the successful execution of your program, ensuring real-time 3D pose estimation of the index finger.

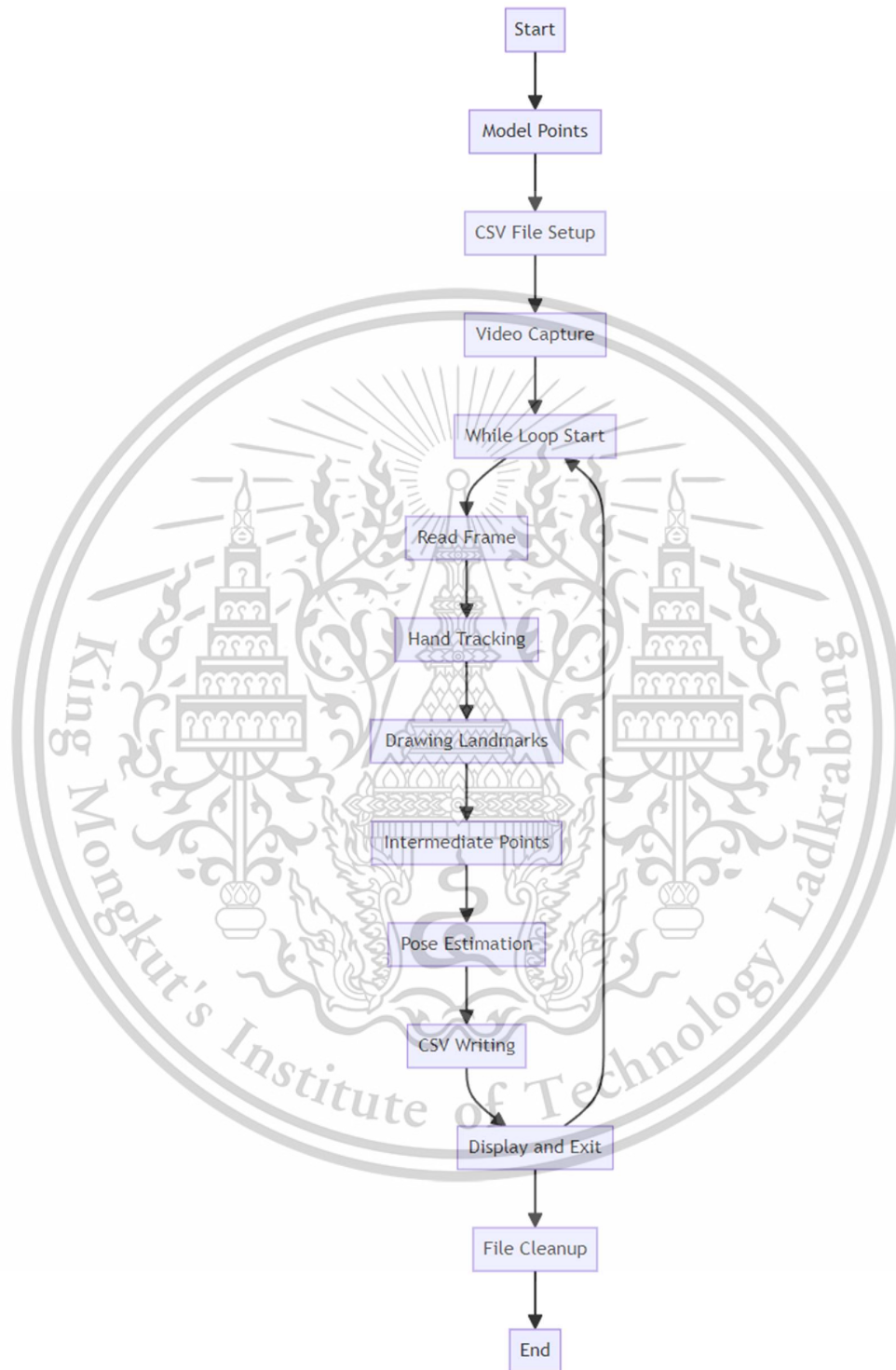


Figure 12 Compute 3D coordinates

This material is reserved for educational use only, not allowed for commercial use.

Forbidden to modify the content, and cite the document when use.

3.4 Calculate kinematic parameter

Utilize the 3D coordinates acquired from the Electromagnetic and Single camera systems that consist of Mediapipe and This research to generate graphs depicting the aperture and transport velocity. Subsequently, compare the graphs to identify any similarities and discrepancies between the patterns observed in the three systems. Down sampling of Electromagnetic from 100 Hz to 60 Hz because of smartphone camera that 60 fps

the distance between the thumb and the index finger tip, referred to as the "aperture," is an important measure. It indicates how wide the hand is opened or how the hand shapes itself when preparing to grasp an object.

$$\text{Aperture} = \sqrt{(x_2 - x_1)^2 + (y_2 - y_1)^2 + (z_2 - z_1)^2}$$

transport velocity of the hand movement, indicating how fast and in which direction the hand is moving at each time step.

$$\text{Transport velocity} = \left(\frac{x_{n+1} - x_n}{\frac{1}{60}} \right) \hat{i} + \left(\frac{y_{n+1} - y_n}{\frac{1}{60}} \right) \hat{j} + \left(\frac{z_{n+1} - z_n}{\frac{1}{60}} \right) \hat{k}$$

3.5 Performance measure

Employing both RMSE and MAE ensures a thorough and balanced evaluation of the Mediapipe and Mediapipe + PnP systems against the Electromagnetic reference. This approach allows you to capture both the overall accuracy and the presence of significant errors, as evident in the provided graph. Both metrics provide valuable insights into how closely the systems' 3D coordinate estimations align with the reference system. The data is numerical and continuous, which is appropriate for RMSE and MAE calculations.

RMSE (Root Mean Square Error): This metric measures the average magnitude of the errors between single camera system values and the actual values (reference data). It is suitable for your data because it helps identify how significant the deviations are, giving more weight to larger errors.

$$\text{RMSE} = \sqrt{\frac{1}{n} \sum_{i=1}^n (y_i - \hat{y}_i)^2}$$

MAE (Mean Absolute Error): This metric measures the average magnitude of the absolute errors between single camera system and the actual values (reference data). It is suitable for your data because it provides a straightforward measure of the average error without squaring the errors, making it easier to interpret.

$$\text{MAE} = \frac{1}{n} \sum_{i=1}^n |y_i - \hat{y}_i|$$

CHAPTER 4

RESULT AND DISCUSSION

4.1 Aperture

Figure shows how well different methods can track the opening and closing of a hand over time. We used three systems to do this: an electromagnetic system, an optical system using MediaPipe, and another optical system using the PnP algorithm.

All three systems showed similar hand movements, which means they are all reliable for this kind of tracking. But we wanted to know which optical system is more accurate, so we looked at two error measurements: RMSE and MAE.

For the PnP algorithm, the RMSE was 0.2115 and the MAE was 0.1412. For MediaPipe, the RMSE was 0.2186 and the MAE was 0.1448. These numbers tell us that the PnP algorithm is slightly more accurate than MediaPipe. So, if you need to be really precise, the PnP algorithm is more accuracy.

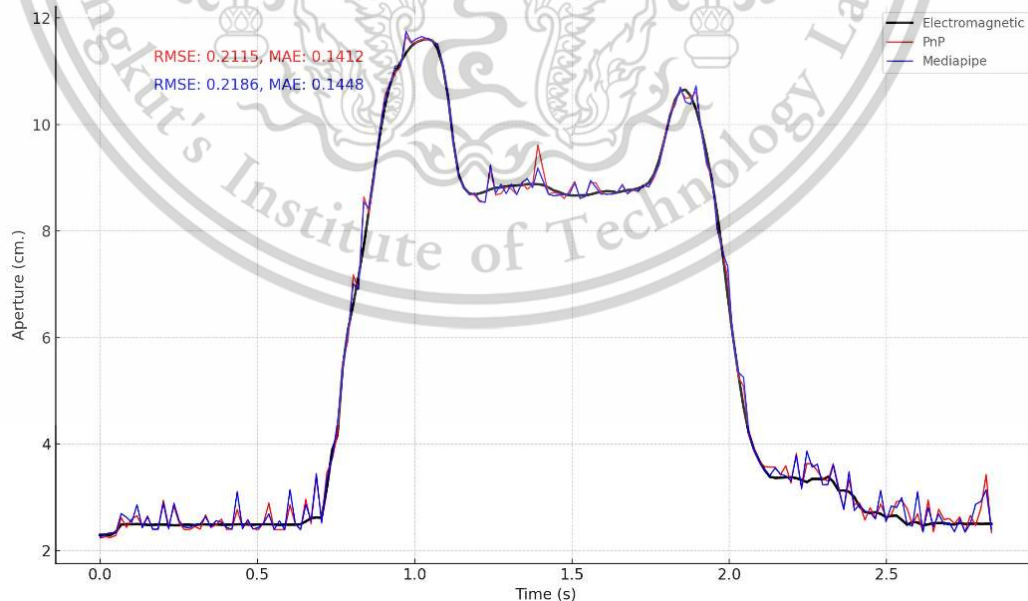


Figure 13 Aperture from three system

4.2 Transport velocity

Figure offers a detailed view of transport velocity of the hand changes over time in this study. We gathered this information by tracking 3D coordinates at a specific point on the wrist, known as the radial stylus, using two different systems. Generally, the hand height patterns from both systems are quite similar, showing only minor differences.

For This research, $RMSE = 0.0291$ and $MAE = 0.0125$. For MediaPipe, $RMSE = 0.0363$ and $MAE = 0.0230$. These results indicate that this research is slightly more accurate than MediaPipe.

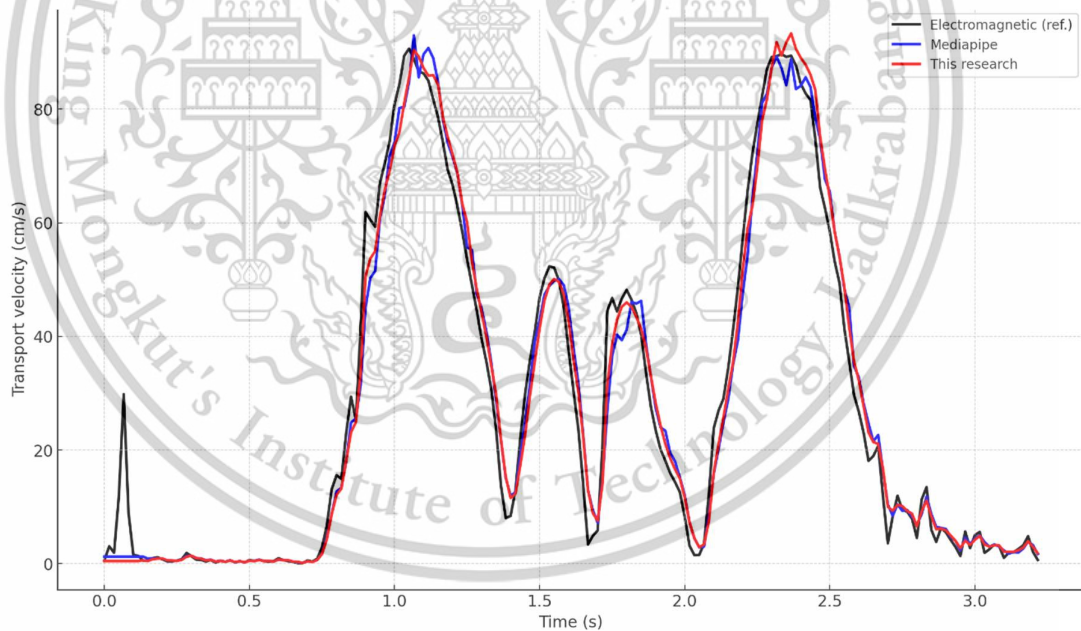


Figure 14 Transport velocity

CHAPTER 5

CONCLUSION AND FUTURE WORK

4.1 Conclusion

The assessment of human movement is a critical aspect of physical therapy management, particularly for evaluating the Reach-to-Grasp (RTG) movement, which is essential for understanding motor skills and therapeutic progress. Traditional Electromagnetic Motion (EM) tracking systems, though highly accurate, are costly and impractical for telemedicine due to their lack of portability and complex setup requirements. This study focuses on developing and implementing a markerless motion tracking system using a single smartphone camera, leveraging the MediaPipe framework and the Perspective-n-Point (PnP) algorithm.

Our research aims to create an accessible, cost-effective, and portable alternative for capturing and analyzing upper extremity movements, specifically the RTG movement. The system is designed to be easy to set up and useful for telemedicine applications, allowing physical therapists to remotely monitor and evaluate patients' motor functions. We conducted a detailed comparison of the kinematic parameters derived from our smartphone-based system with those obtained from a standard EM tracking system to assess performance and accuracy.

The findings suggest that the single smartphone camera system, utilizing MediaPipe and the PnP algorithm, can effectively provide reliable and accurate 3D pose estimations. The kinematic parameters, such as aperture and transport velocity, obtained from our system are comparable to those from the EM tracking system. This indicates that the smartphone-based system can serve as a practical and accessible tool for telemedicine applications, potentially transforming the way physical therapy is delivered and expanding access to healthcare for patients in remote or underserved areas.

4.2 Limitation and Future work

Limitation of this study (Pnp algorithm) is the detection and tracking accuracy of the system are dependent on the performance of the MediaPipe framework. Any limitations or inaccuracies inherent in MediaPipe's hand detection and pose estimation capabilities will directly impact the overall effectiveness of the motion tracking system developed in this study. For our next steps, we plan to make our motion capture system even better. One idea is to add more cameras to capture different angles, which could make the tracking more accurate. We're also thinking about testing our system in real-world settings, like hospitals or rehab centers, to see how well it works outside the lab. Another important area we want to explore is making the system easier to use, so that even people without technical skills can set it up. Lastly, we're interested in seeing how our system performs when tracking other types of movements, not just Reach-to-Grasp. By tackling these areas, we hope to make our system more useful for a wider range of people and situations.



REFERENCES

- [1] H. Zhou and H. Hu, "Human motion tracking for rehabilitation – A survey," *Biomed. Signal Process.*, vol. 3, no.1, pp. 1-18, Jan. 2008.
- [2] S. Rungseethanakul, J. Tretriluxana, P. Piriyaprasarth, N. Pakaprot, K. Jitaree, S. Tretriluxana, and J.V. Danoff. "Task oriented training activities post stroke will produce measurable alterations in brain plasticity concurrent with skill improvement," *Top. Stroke Rehabil.*, vol. 22, no. 4, pp.241-254, 2022 doi:10.1080/10749357.2021.1926136
- [3] J. Thanakamchokchai, J. Tretriluxana, N. Pakaprot, A. Pisarnpong and B.E. Fisher "Effects of high-frequency repetitive transcranial magnetic stimulation on reach-to-grasp performance in individuals with Parkinson's disease: a preliminary study," *Exp. Brain Res.*, vol. 238, pp.1827-1837, 2020.
- [4] N. J. Jarque-Bou, M. Atzori and H. Muller, "A large calibrated database of hand movements and grasps kinematics," *Sci. Data.*, vol.7, no.1, doi: 10.1038/s41597-019-0349-2, Jan. 9, 2020.
- [5] A.D. Milne, D.G. Chess, J.A. Johnson and G.J.W. King "Accuracy of an Electromagnetic Tracking Device: A Study of the Optimal Operating Range and Metal Interference," *J. Biomech.*, vol. 29, no.6, pp 791-793, June 1996.
- [6] S. LaScalza, J. Arico and R. Hughes "Effect of metal and sampling rate on accuracy of Flock of Birds electromagnetic tracking system," *J. Biomech.*, vol. 36, no.1, pp 141-144, 2003.
- [7] The MotionMonitor by Innovative Sports Training, Inc. available at <https://www.innsport.com/>, Accessed on March 10, 2022.
- [8] N. Runnarong, J. Tretriluxana, W. Waiyasil, P. Sittisupapong, and S. Tretriluxana. "Age-related Changes in Reach-to-grasp Movements with Partial Visual Occlusion," *Plos One* <https://doi.org/10.1371/journal.pone.0221320>, 2019.
- [9] J. Tretriluxana, J. Thanakamchokchai, C. Jalayondeja, N. Pakaprot, and S. Tretriluxana. "The Persisted Effects of Low-Frequency Repetitive Transcranial Magnetic Stimulation to Augment Task-Specific Induced Hand Recovery Following Subacute Stroke: Extended Study," *Ann Rehabil Med.*, vol. 42, no.6, pp.777-787, 2018.

- [10] J. Tretriluxana, S. Kantak, S. Tretriluxana, A.D. Wu, and B.E. Fisher. "Improvement in Paretic Arm Reach-to-grasp Following Low Frequency Repetitive Transcranial Magnetic Stimulation Depends on Object Size: A Pilot Study," *Stroke Res. Treat*, 2015.
- [11] J. Tretriluxana, R. Vachalathiti, N. Runnarong, S. Tretriluxana, N. Prayoonwiwat, and C.J. Winstein. "Feasibility Investigation of the Accelerated Skill Acquisition Program (ASAP): Insights into Reach-to-grasp Coordination of Individuals with Postacute Stroke," *Top. Stroke Rehabil.*, vol. 20, no.2, pp.151–160, 2013
- [12] J. Tretriluxana, S. Kantak, S. Tretriluxana, A.D. Wu, and B.E. Fisher. "Low Frequency Repetitive Transcranial Magnetic Stimulation to the Non-lesioned Hemisphere Improves Paretic Arm Reach-to-grasp Performance after Chronic Stroke," *Disabil. Rehabil.: Assist. Technol.*, vol. 8, no.2, pp.121–124, 2013.
- [13] C. Tan, J. Tretriluxana, E. Pitsch, N. Runnarong, and C.J. Winstein. "Anticipatory Planning of Functional Reach-to-grasp: A Pilot Study," *Neurorehabil Neural Repair.*, vol. 26, no 8, pp.957-967, 2012.
- [14] MathWorks, (2022). *Image Processing Toolbox: User's Guide (R2022a)*. Retrieved April 12, 2022 from https://www.mathworks.com/help/pdf_doc/images/images Ug.pdf
- [15] Urbanczyk CA, Bonfiglio A, McGregor AH, Bull AMJ. Comparing optical and electromagnetic tracking systems to facilitate compatibility in sports kinematics data. *Int Biomech.* 2021 Dec;8(1):75-84. doi: 10.1080/23335432.2021.2003719. PMID: 34806553; PMCID: PMC8635616.
- [16] Wanbin Tan et al. Wearable electromagnetic motion tracking with submillimeter accuracy: an experimental study using high-resolution Prism-PET brain scanner *Journal of Nuclear Medicine* August 2022, 63 (supplement 2) 3320
- [17] Amosa T.I. et al. Multi-camera multi-object tracking: a review of current trends and future advances *Neurocomputing* (2023)
- [18] Pottorf O, Vapne D, Ghigiarelli J, Haase K. Reliability and Concurrent Validity of a Markerless, Single Camera, Portable 3D Motion Capture System for Assessment of Glenohumeral Mobility. *IJSPT.* 2023;18(5):1176-1185. doi:10.26603/001c.88003

[19] Zhang, F.; Bazarevsky, V.; Vakunov, A.; Tkachenka, A.; Sung, G.; Chang, C.-L.; Grundmann, M. Mediapipe Hands: On-Device Real-Time Hand Tracking. arXiv 2020, arXiv:2006.10214

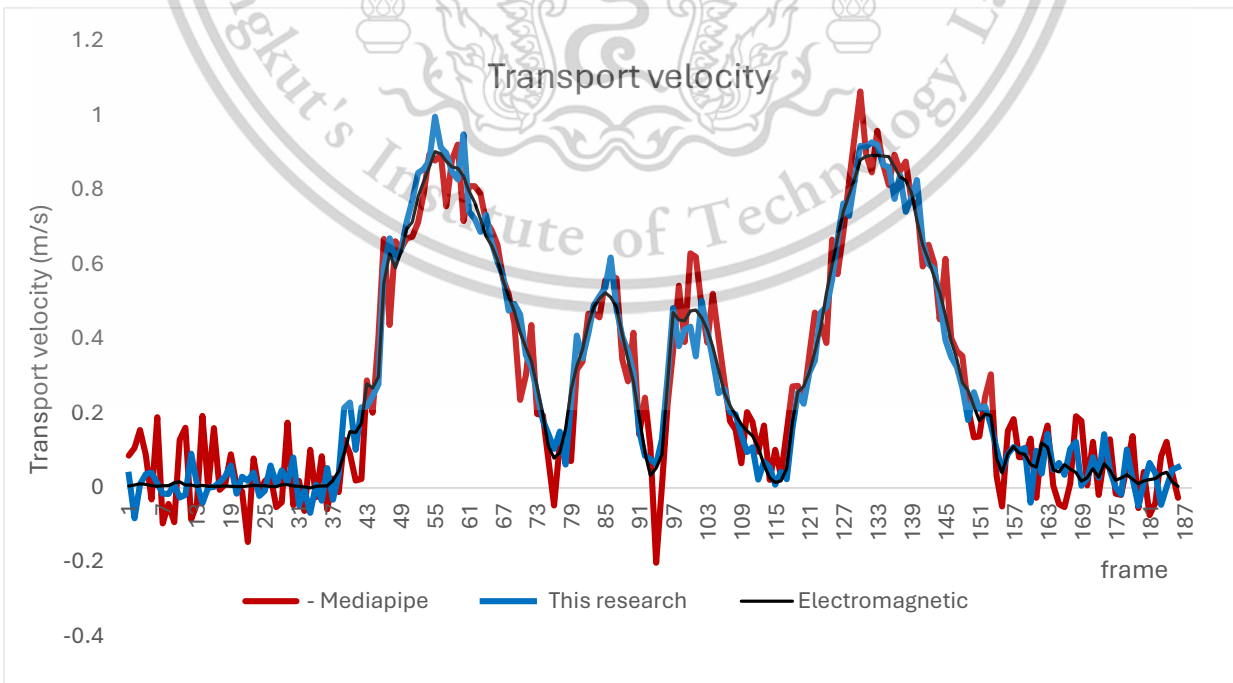
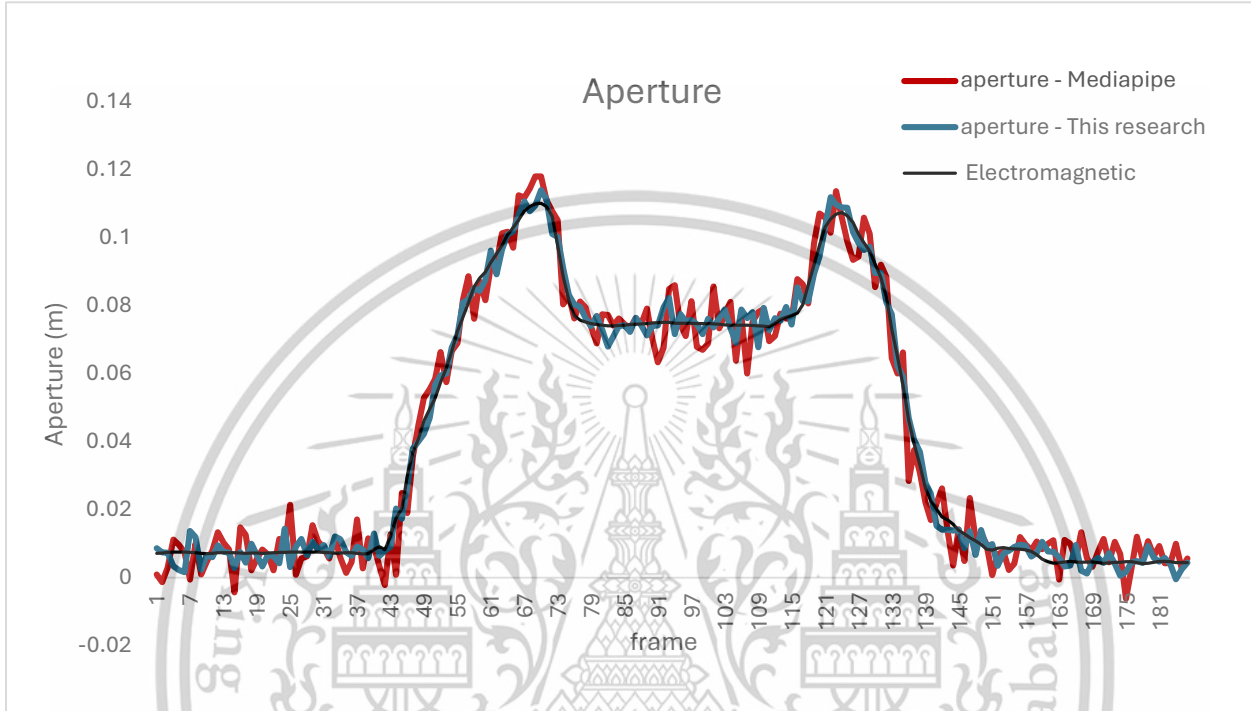
[20] Fischler, M. A.; Bolles, R. C. (1981). "Random Sample Consensus: A Paradigm for Model Fitting with Applications to Image Analysis and Automated Cartography". *Communications of the ACM*. 24 (6): 381–395. doi:10.1145/358669.358692. S2CID 972888.





This material is reserved for educational use only, not allowed for commercial use.

Forbidden to modify the content, and cite the document when use.



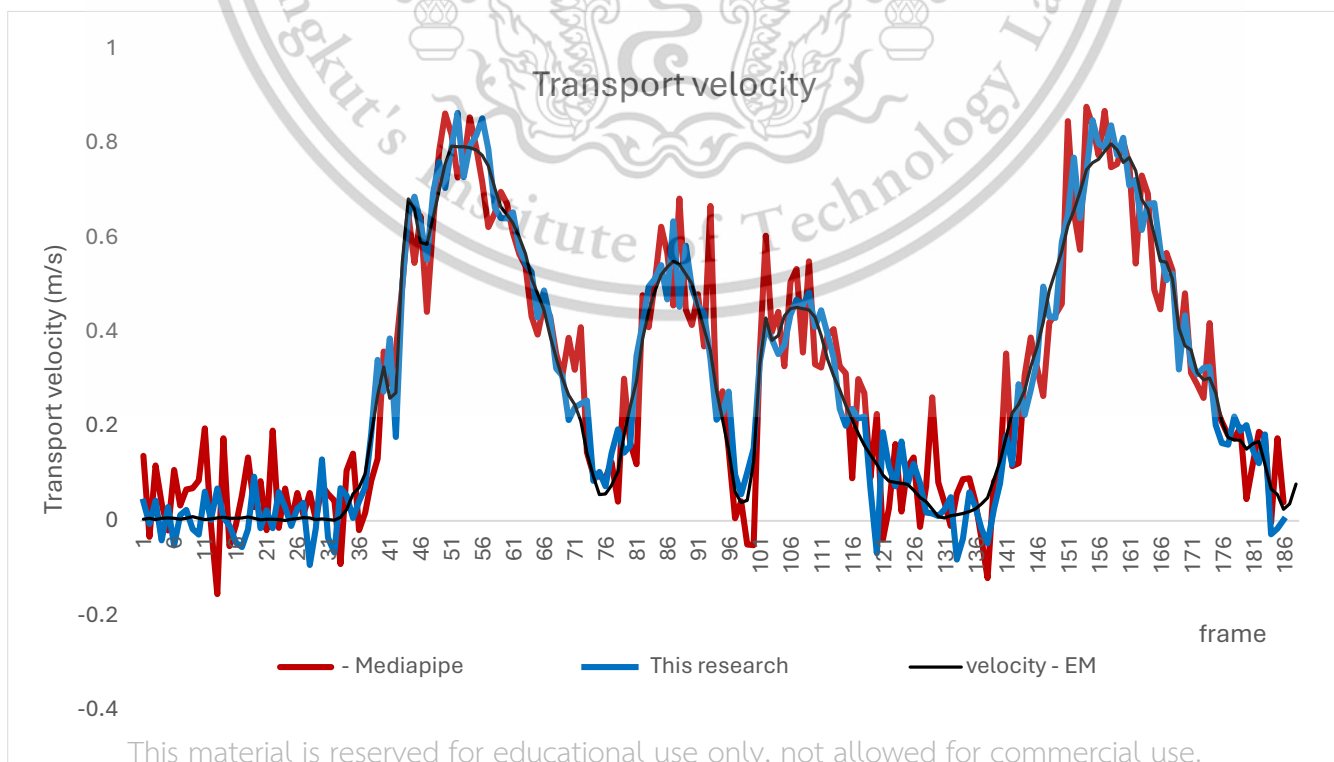
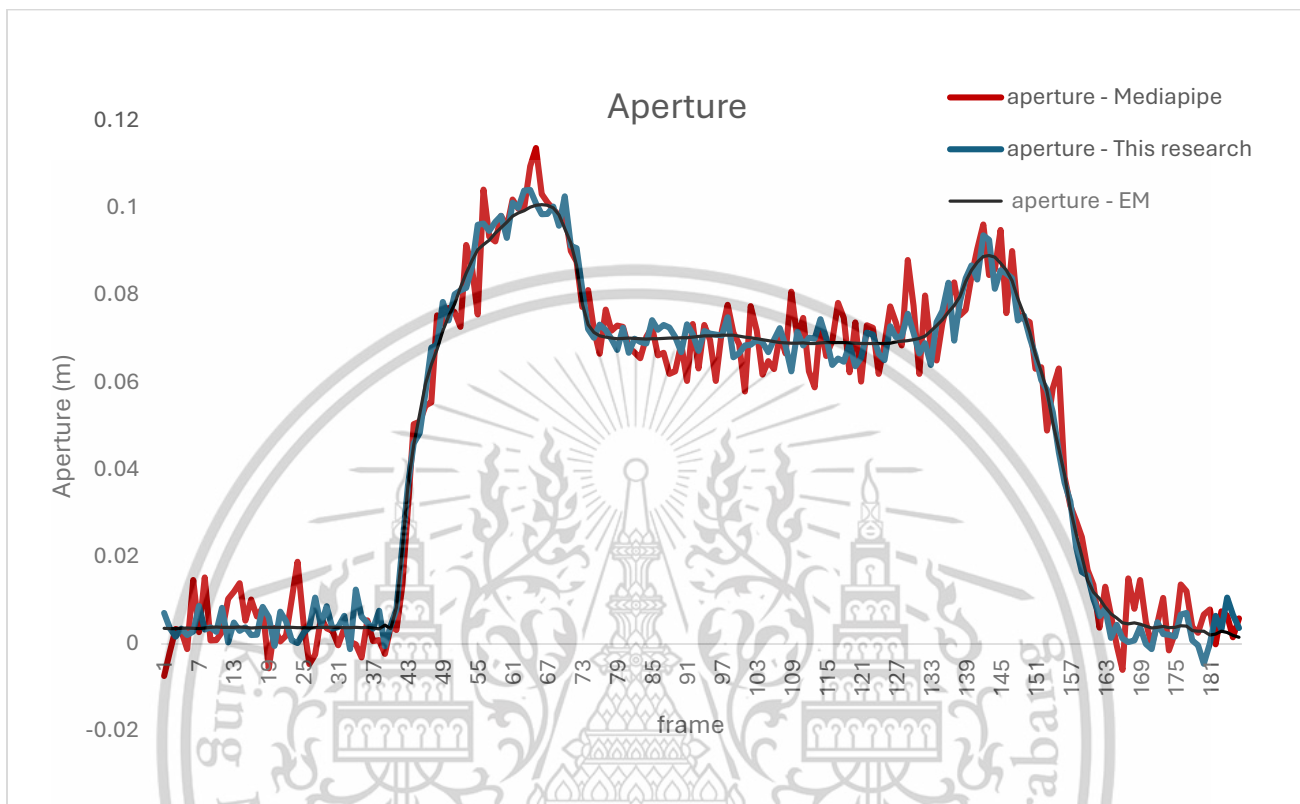
This material is reserved for educational use only, not allowed for commercial use.

Forbidden to modify the content, and cite the document when use.

Table 2 Result from trial2

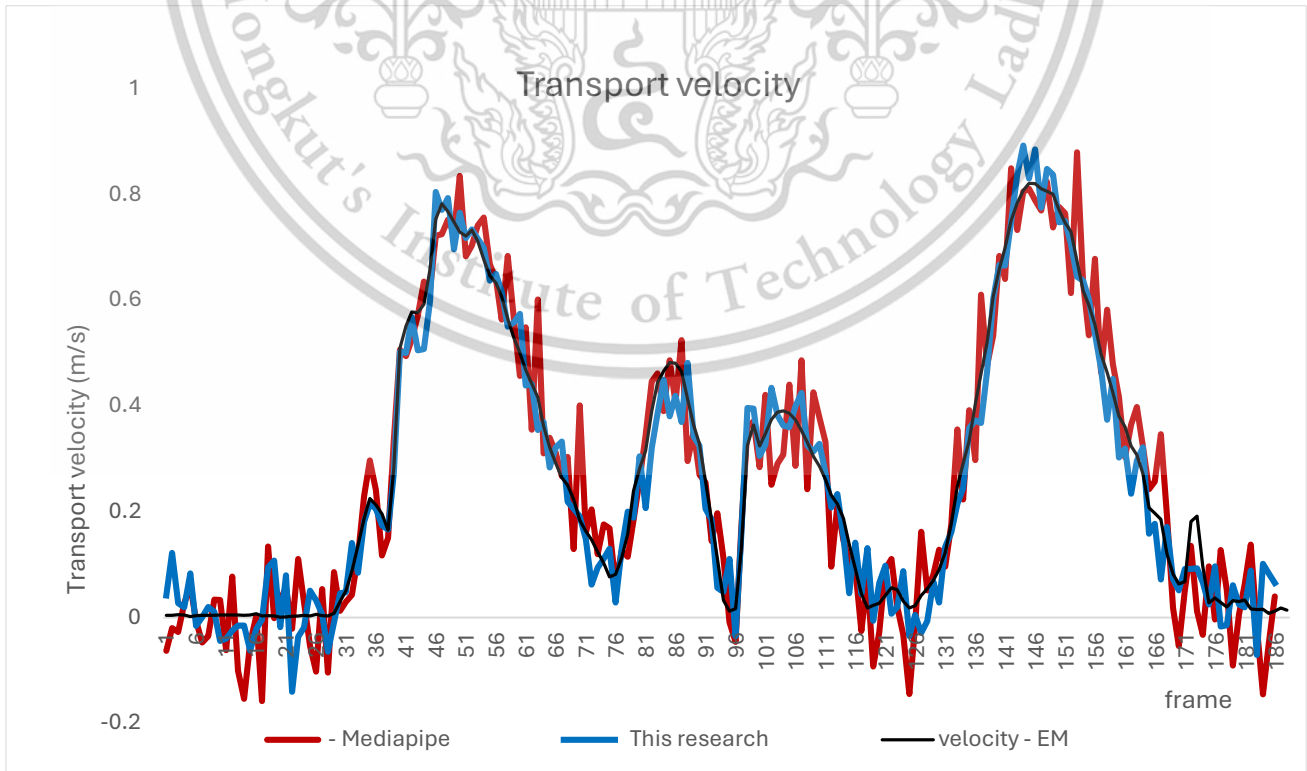
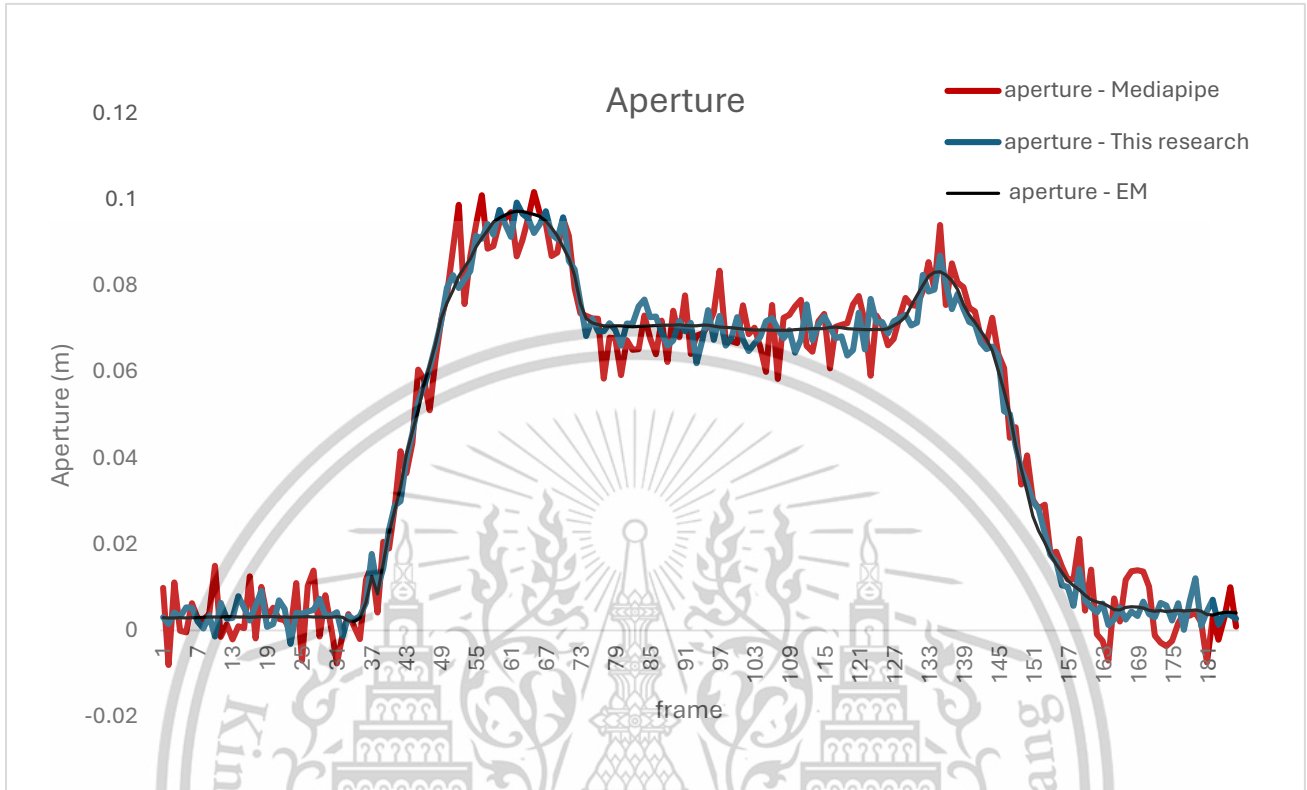
frame	velocity - EM	aperture - EM	This research	aperture - This research	Mediapipe	aperture - Mediapipe
1	0.0035985	0.003537	0.004046521	0.007098059	0.137446117	-0.007367924
2	0.005277	0.003498	0.006963419	0.003537085	0.033716382	-0.001813061
3	0.0027115	0.0034715	0.0042510527	0.001632468	0.117408093	-0.003448935
4	0.0056715	0.0035865	-0.041239678	0.003492305	0.007601263	0.002899757
5	0.005842	0.003653	0.0029235744	0.00205422	-0.020686191	-0.001195342
6	0.005547	0.003541	-0.052283929	0.002822445	0.107998108	0.01468178
7	0.003667	0.0034755	-0.112310893	0.00689404	0.032603617	0.002710657
8	0.005697	0.003652	0.023119897	0.003282625	0.066707011	0.01526879
9	0.0085575	0.0038095	-0.017370084	0.003791838	0.069107172	0.000800608
10	0.0050725	0.0038205	-0.293931798	0.002787103	0.085447294	0.000838102
11	0.002517	0.003779	0.061656549	0.002821617	0.196220346	0.002764888
12	0.0044475	0.003773	0.001762347	0.006397288	-0.004852595	0.013379704
13	0.006095	0.0037495	0.06369893	0.004898959	0.155340534	0.011932321
14	0.007457	0.003824	0.007714781	0.002941661	0.175379146	0.013916844
15	0.0050625	0.003784	0.10052122	0.003793952	-0.053420063	0.002079795
16	0.005725	0.003643	0.002035472	0.002033475	-0.008607799	0.015292556
17	0.006351	0.003722	0.055646292	0.00282335	0.054367253	0.006294772
18	0.008375	0.003783	-0.117958012	0.008483867	0.134564885	0.006275132
19	0.0055355	0.0037505	0.093287597	0.006107058	0.29039610	-0.005653892
20	0.002069	0.00376	-0.015592253	-0.000452084	0.083961021	0.003610938
21	0.0031745	0.003793	0.022314624	0.007359111	-0.019078743	0.005387991
22	0.0032825	0.003781	-0.115879005	0.005215334	0.191395455	-0.00188995
23	0.002396	0.00375	0.061373704	0.000784582	-0.015261727	0.01038567
24	0.001099	0.0037315	0.028438928	0.000175511	0.06863272	0.01883668
25	0.0031205	0.003683	-0.011068979	0.00254956	-0.001382466	0.004529541
26	0.005003	0.003657	0.026534062	0.003822584	0.059121212	-0.004697202
27	0.006603	0.003715	0.037676803	0.010610955	0.001724898	-0.020283237
28	0.0051095	0.0038085	0.039415649	0.004231871	0.005806952	0.005868255
29	0.0020626	0.003807	-0.014639913	0.006819454	0.002655889	-0.035988929
30	0.004221	0.0037665	0.130332182	0.003504809	0.014978593	-0.002010351
31	0.0024935	0.003749	-0.030651128	0.003873965	0.056791472	-0.002098033
32	0.001305	0.003705	0.066975797	0.006396627	0.042906622	0.003551763
33	0.0071585	0.0037055	0.068971185	0.001202827	-0.091363986	0.000481036
34	0.0239	0.0037515	0.053770797	0.01248356	0.106754304	-0.001212499
35	0.056738	0.003704	0.006166591	0.006199248	0.146272243	-0.003152441
36	0.070393	0.0038125	0.041573628	0.004838703	0.019761549	0.005381433
37	0.0996575	0.0036545	0.007123231	0.003509541	0.016926743	0.000606101
38	0.182132	0.003385	0.184610363	0.007630552	0.084617865	0.000817129
39	0.266225	0.0043215	0.341495222	-0.000542845	0.1316963	-0.002346626
40	0.326251	0.0034635	0.274456839	0.004174625	0.359124738	0.004007343
41	0.260218	0.00832	0.3688112	0.00790074	0.290515315	0.003200201
42	0.2717115	0.021458	0.177452823	0.022169232	0.361446096	0.013191866
43	0.547997	0.036429	0.499323935	0.036451265	0.496641579	0.031202787
44	0.628355	0.045694	0.649786509	0.046041388	0.649694208	0.050423466
45	0.6607115	0.0528785	0.687443598	0.048745408	0.45725551	0.051075103
46	0.590675	0.0598045	0.633879224	0.057882064	0.646206228	0.0542615
47	0.586543	0.064131	0.553659377	0.068205707	0.443011022	0.052462964
48	0.641808	0.067651	0.693634111	0.068701092	0.627290414	0.075439634
49	0.6995675	0.071906	0.761394968	0.078556269	0.783165874	0.073568849
50	0.757259	0.075259	0.705594791	0.074263864	0.838350306	0.077122559
51	0.794949	0.078112	0.792739091	0.080328968	0.819184244	0.067260515
52	0.793097	0.0818085	0.865599897	0.081658683	0.782206007	0.072770269
53	0.793328	0.085164	0.728673237	0.081766905	0.757749345	0.091579378
54	0.790934	0.0880305	0.794403089	0.085523286	0.85544998	0.086457998
55	0.78675	0.090542	0.816807754	0.096226139	0.791833655	0.075865624
56	0.774923	0.091707	0.85362981	0.096542377	0.719771182	0.1043056
57	0.752804	0.0927475	0.787577555	0.094843511	0.622720131	0.093519737
58	0.7056925	0.093432	0.665348564	0.096884782	0.657196424	0.092461744
59	0.655437	0.095547	0.64167028	0.096204138	0.678476684	0.097876684
60	0.64914	0.0968385	0.641347853	0.09321493	0.673118934	0.096761892
61	0.630996	0.0982605	0.654134299	0.093131208	0.610144845	0.102023205
62	0.600461	0.098974	0.578399394	0.100128105	0.562576559	0.099914713
63	0.5665705	0.0995035	0.545910889	0.104077414	0.54063384	0.100027095
64	0.513822	0.100263	0.527756769	0.104318576	0.433502601	0.109724095
65	0.481712	0.100732	0.430606638	0.101892277	0.394789886	0.113928226
66	0.446552	0.1009065	0.488691245	0.09864221	0.46044124	0.103371131
67	0.391948	0.1007465	0.428761651	0.098737267	0.433721763	0.101356656
68	0.345222	0.100108	0.322663658	0.10046492	0.324308648	0.0998528
69	0.302374	0.0985445	0.308216541	0.096004135	0.306903833	0.098391892
70	0.266406	0.0953295	0.231395607	0.102768343	0.388050059	0.099144736
71	0.246084	0.092058	0.240103722	0.091398304	0.320614395	0.092049536
72	0.211871	0.0868375	0.244144411	0.090878638	0.310397768	0.087815178
73	0.144167	0.080705	0.25479062	0.081274338	0.148943913	0.077319626
74	0.094668	0.07328	0.084597568	0.07250739	0.09898644	0.081228368
75	0.055641	0.0715845	0.103578636	0.070325955	0.093931149	0.071328694
76	0.057155	0.070763	0.073207842	0.07279415	0.090954487	0.065664383
77	0.075402	0.070412	0.142924933	0.072092248	0.124159567	0.076733361
78	0.104202	0.0701965	0.143343888	0.07002335	0.104061075	0.071928218
79	0.1810165	0.0700815	0.144416263	0.067531521	0.103135006	0.073109373
80	0.241718	0.070173	0.158511214	0.072589937	0.166093702	0.072799429
81	0.2961185	0.070285	0.350130284	0.066878649	0.11975478	0.068068365
82	0.3861715	0.070157	0.318718188	0.070111021	0.078520048	0.066955344
83	0.442924	0.070073	0.496974877	0.069355443	0.104003606	0.06613381
84	0.486657	0.070042	0.512889146	0.069013003	0.503802741	0.070536505
85	0.5220865	0.0700565	0.541905458	0.074333588	0.623463285	0.072717426
86	0.538228	0.070071	0.469628655	0.072136007	0.568931949	0.06281996
87	0.550669	0.0701275	0.635424921	0.072523753	0.465653082	0.066830182
88	0.543213	0.0702165	0.463981047	0.072639421	0.683202629	0.062051298
89	0.522994	0.070253	0.583358919	0.070539787	0.447701948	0.062588663
90	0.5027165	0.0702675	0.495011484	0.07041182	0.415238844	0.066921872
91	0.453207	0.07032	0.455762897	0.070339538	0.480392009	0.063413641
92	0.407418	0.070444	0.440975533	0.071144821	0.369888244	0.073472644
93	0.3604695	0.070583	0.430470823	0.067283997	0.667777882	0.063230161
94	0.275702	0.070718	0.214129554	0.071826119	0.235560171	0.073230112
95	0.214102	0.07076	0.0259571725	0.071239852	0.274644562	0.069779613
96	0.1502595	0.070725	0.273911211	0.071041463	0.150656756	0.060351082
97	0.061543	0.0708735	0.098678325	0.070803445	0.005468202	0.071898257
98	0.038754	0.070874	0.056487106	0.07500576	0.061489576	0.077863548
99	0.04357	0.070854	0.102760127	0.065806016	-0.050458883	0.071451838
100	0.124831	0.070695	0.152399262	0.066759985	-0.051782392	0.068837118
101	0.330651	0.070473	0.335198887	0.06854605	0.352283974	0.057974688
102	0.430195	0.070316	0.409925982	0.06689917	0.604398906	0.077544721
103	0.382657	0.0700845	0.385274731	0.069753744	0.400528248	0.071948825
104	0.392885	0.069857	0.35363473	0.069222348	0.443102976	0.061866474
105	0.434172	0.0696885	0.372738959	0.06989699	0.327738959	0.064949118
106	0.450096	0.069402	0.463089097	0.06985827	0.05840374	0.06317191
107	0.452618	0.06932	0.46995955	0.072470393	0.53939404	0.070985054
108	0.449744	0.0691415	0.45635754	0.068433539	0.35687589	0.067010339
109	0.4472595	0.0690325	0.484405444	0.06259597	0.55004604	0.080851362
110	0.431826	0.069061	0.411194735	0.071715903	0.331510043	0.070662664
111	0.3931745	0.0690295	0.44645351	0.068546324	0.324879995	0.074887236
112	0.3424225	0.0689665	0.389650385	0.070322529	0.393170401	0.065264318
113	0.307174	0.06896	0.345062732	0.070073738	0.406689854	0.058902827

114	0.277947	0.069103	0.23764317	0.074561641	0.328026284	0.073687993
115	0.245018	0.0691905	0.201546091	0.070245393	0.312861854	0.06613796
116	0.214554	0.069163	0.237385243	0.064044405	0.089956408	0.069562486
117	0.185522	0.069186	0.216893527	0.063486006	0.300387606	0.07288421
118	0.1600255	0.069194	0.22116018	0.064807765	0.270571645	0.074823251
119	0.140025	0.069132	0.068571846	0.068852592	0.210282454	0.062375



This material is reserved for educational use only, not allowed for commercial use.

Forbidden to modify the content, and cite the document when use.

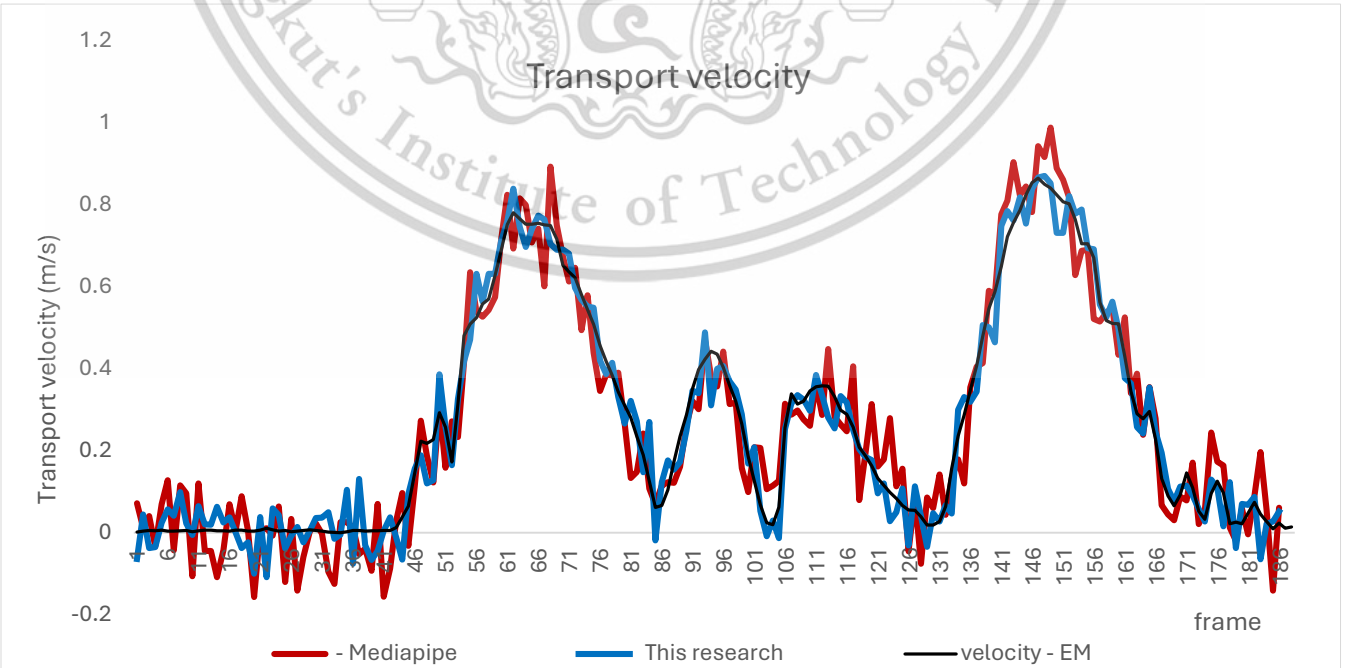
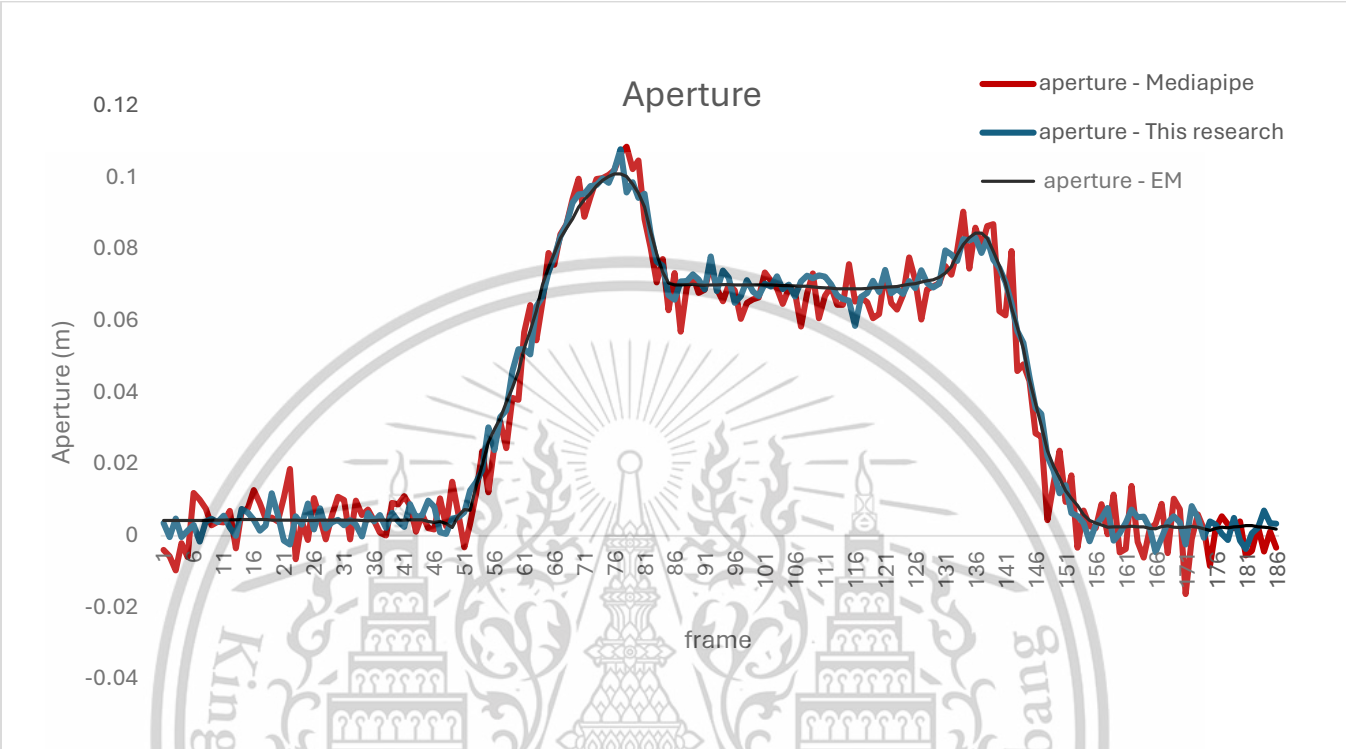


This material is reserved for educational use only, not allowed for commercial use.

Forbidden to modify the content, and cite the document when use.

Table 4 Result from trial4

frame	velocity - EM	aperture - EM	This research	aperture - This research	- Mediapipe	aperture - Mediapipe
1	0.0012895	0.004273	-0.064205476	0.003521921	0.071532986	-0.004040171
2	0.003771	0.004238	0.04433661	-0.000415715	0.012560125	-0.005766794
3	0.0055285	0.004208	-0.038082795	0.004759206	0.040033297	-0.009760607
4	0.0042485	0.004206	-0.035866789	-0.000377156	-0.034120669	-0.002135
5	0.005901	0.00421	0.024125053	0.001406899	0.069015538	-0.005983284
6	0.0032275	0.004206	0.056458964	0.003006824	0.127673873	0.011947114
7	0.003715	0.004204	0.040940467	-0.001656116	-0.043202629	0.010015199
8	0.004634	0.00423	0.098881338	0.003978515	0.11532372	0.005765554
9	0.0052195	0.004285	0.022757168	0.004713534	0.095535361	0.00292624
10	0.002246	0.00433	-0.005483282	0.003804309	-0.106836592	0.003895163
11	0.004229	0.00435	0.064812855	0.00561404	0.119925901	0.003686111
12	0.006197	0.004375	0.019679037	0.002230066	-0.044569971	0.006874405
13	0.006054	0.0044265	0.018917165	-2.658595E-05	-0.044552713	-0.003512967
14	0.004612	0.004484	0.062802469	0.007416163	-0.109164048	0.006762479
15	0.0042525	0.0045	0.02448833	0.006440286	-0.042985864	0.007560928
16	0.0034285	0.0045005	0.037132979	0.004390631	0.069496787	0.01271465
17	0.005636	0.004508	0.000762753	0.014081474	0.004609105	0.009041235
18	0.0063295	0.004474	-0.037861455	0.002793977	0.089117468	0.004747327
19	0.003965	0.0043555	-0.023487679	0.01187966	0.004668972	0.005030621
20	0.00373	0.00432	-0.100259964	0.005801185	-0.157397608	0.003980899
21	0.0060835	0.004328	0.03791402	-0.001411345	0.006268448	0.010698737
22	0.010569	0.004337	-0.108245888	-0.002495631	0.010891579	0.018635368
23	0.006701	0.004331	0.059505628	0.005370422	-0.007535721	-0.006587158
24	0.003372	0.004267	0.042377067	0.003109346	0.0641615	0.003928163
25	0.004819	0.0042095	-0.038571111	0.00898923	-0.120793238	-0.001267128
26	0.002332	0.004256	-0.007840715	0.001701748	0.03594155	0.010525101
27	0.0034975	0.0042935	0.014135953	0.007630859	-0.142184301	0.004767369
28	0.005067	0.004315	-0.023837864	0.001959926	-0.09521227	-0.001107014
29	0.006066	0.0043	0.004057163	0.00373518	0.002792212	0.005536997
30	0.00517	0.004279	0.035591144	0.004372202	0.02227874	0.010815334
31	0.00382	0.004313	0.03264265	0.00292775	-0.00262706	0.009931759
32	0.001636	0.004352	0.050037147	0.004332859	-0.095803543	-0.001005917
33	0.004007	0.0043485	-0.014949896	0.003043585	-0.125665628	0.009786881
34	0.0009975	0.004245	-0.004620291	-0.000231995	0.025339556	0.005729455
35	0.001835	0.004153	0.104634781	0.006294355	0.025325272	0.00729122
36	0.0047935	0.0042285	-0.076030089	0.00400787	0.012785114	0.004158535
37	0.0048605	0.0042975	0.131152594	0.005749556	-0.052815486	0.000847243
38	0.003892	0.004293	-0.038000058	0.002146139	-0.039078463	-4.31208E-05
39	0.0043835	0.0042915	-0.067066589	0.006386163	-0.09359182	0.009174684
40	0.004091	0.0043065	-0.044599048	0.004065218	0.070409182	0.008698745
41	0.005301	0.004329	0.004723114	0.002476617	-0.156780884	0.011059899
42	0.0053035	0.0043685	0.037321959	0.008807904	-0.088083499	0.008399779
43	0.0125725	0.0044265	-0.011677929	0.005136272	0.02865983	0.00110159
44	0.030854	0.004392	-0.065974029	0.005677623	0.096592213	0.0059185
45	0.0645945	0.0039485	0.094044453	0.009807008	-0.032015396	0.002067089
46	0.146074	0.0036875	0.156365982	0.008087605	0.114197005	0.001710092
47	0.223122	0.00398	0.188818349	0.000893213	0.273159756	0.010407534
48	0.2177285	0.003354	0.119877721	0.000508474	0.187535449	0.00257586
49	0.226862	0.0022805	0.127555453	0.004793517	0.122475767	0.015019664
50	0.292654	0.005448	0.386422622	0.005157888	0.310500285	0.006241782
51	0.2579145	0.007315	0.258327951	0.006522871	0.158413636	-0.00323905
52	0.1723675	0.007136	0.16461375	0.012671006	0.271638967	0.003297902
53	0.314994	0.013933	0.326792108	0.014954323	0.233482495	0.011797003
54	0.481227	0.019811	0.418922484	0.019837612	0.415449645	0.023539394
55	0.509117	0.026179	0.471141061	0.030249101	0.636475734	0.012092871
56	0.525284	0.029769	0.632362009	0.032958023	0.539261599	0.02525282
57	0.585811	0.03279	0.563978506	0.03163987	0.527517192	0.031863059
58	0.5705575	0.0372915	0.632391928	0.034972797	0.543891206	0.024468516
59	0.628239	0.041297	0.631906201	0.045924697	0.57497824	0.038519399
60	0.689476	0.0459275	0.712440129	0.052144303	0.716036471	0.037925312
61	0.7526205	0.052404	0.75979546	0.052098527	0.825501316	0.056830496
62	0.781927	0.057303	0.840287836	0.050651332	0.694147536	0.06444588
63	0.66962	0.062829	0.747509301	0.064071256	0.816840081	0.054572818
64	0.7531735	0.0700885	0.697688338	0.066750621	0.800436605	0.065269547
65	0.753672	0.074932	0.741470374	0.073078483	0.709082913	0.079037431
66	0.75593	0.078874	0.774885392	0.077891511	0.742424561	0.075767305
67	0.7516115	0.0831895	0.764831775	0.083633996	0.601594454	0.084271128
68	0.750095	0.085964	0.705001992	0.086950004	0.894440885	0.086971656
69	0.7164035	0.0885175	0.691283362	0.093112514	0.749979217	0.094087851
70	0.653339	0.091824	0.691576811	0.095407592	0.675134307	0.099767134
71	0.636779	0.093997	0.681163771	0.095620953	0.613543695	0.089127405
72	0.622983	0.095714	0.597942011	0.09776554	0.646878974	0.09473672
73	0.581324	0.097856	0.568675661	0.09799273	0.494921896	0.099740564
74	0.544554	0.099375	0.552803614	0.099923771	0.579990982	0.100016626
75	0.5085225	0.1004315	0.549042604	0.098608828	0.439068881	0.098663318
76	0.457381	0.101188	0.420545007	0.102439182	0.346162302	0.102193932
77	0.419026	0.101183	0.387748064	0.108114932	0.386304659	0.106848221
78	0.38427	0.100419	0.415072768	0.095970674	0.384108159	0.108812098
79	0.3438185	0.0982855	0.330996609	0.098834052	0.390271765	0.102469664
80	0.311104	0.095743	0.266001244	0.094456589	0.266705599	0.104895583
81	0.281357	0.0919715	0.321862442	0.095597166	0.133339099	0.088569884
82	0.2352875	0.0850575	0.271494954	0.084599808	0.148004036	0.080534658
83	0.189974	0.078761	0.147163401	0.076612503	0.241987252	0.070777161
84	0.1255685	0.0736285	0.27037941	0.075500229	0.107361101	0.07734151
85	0.0618095	0.0706325	-0.018910329	0.067227559	0.06905641	0.06301595
86	0.066353	0.0701	0.123240369	0.065961899	0.114604705	0.07340257
87	0.104261	0.0700635	0.176200122	0.071064462	0.122881949	0.057056419
88	0.173286	0.0701885	0.153353176	0.071170245	0.121364696	0.069485433
89	0.234656	0.070229	0.172140619	0.073014002	0.16102755	0.072795897
90	0.2874565	0.070058	0.248890787	0.071590958	0.263205482	0.067879805
91	0.3517135	0.070001	0.346515017	0.068852247	0.320822672	0.06878821
92	0.398192	0.070081	0.340376114	0.078087546	0.301456031	0.075913123
93	0.4238555	0.0701265	0.488792618	0.0668380917	0.470620659	0.069025006
94	0.4434165	0.070215	0.310809627	0.074128191	0.38245611	0.065499819
95	0.435786	0.070216	0.400246003	0.072178315	0.357373008	0.070053595
96	0.4039615	0.070131	0.406715348	0.065076343	0.441863886	0.068576059
97	0.3596885	0.070136	0.369506607	0.066971415	0.314281693	0.060624055
98	0.321225	0.070124	0.349402339	0.071422694	0.317471215	0.065120295
99	0.2653505	0.0700535	0.289070728	0.068255457	0.157895873	0.066107236
100	0.1861475	0.070051	0.168231783	0.066944375	0.098832441	0.066611636
101	0.126172	0.070114	0.208646254	0.070407507	0.208417954	0.07357716
102	0.0677345	0.0701345	0.0530915	0.069651755	0.207039918	0.07125211
103	0.0237555	0.070042	-0.0090606	0.072499134	0.106304316	0.069089086
104	0.019526	0.069957	0.029503994	0.068889415	0.11453563	0.06482743
105	0.062573	0.0699015	-0.013254739	0.070177558	0.126119839	0.069114511
106	0.25578	0.0698075	0.25328859	0.066870334	0.31497119	0.068135135
107	0.339366	0.06977	0.315243676	0.071072867	0.288503747	0.058479119
108	0.3142595	0.0697405	0.336046087	0.072687711	0.298762477	0.067699336
109	0.3207295	0.069535	0.324989587	0.071953954	0.276439593	0.073358587
110	0.34622	0.069374	0.2976983	0.0728006	0.260474622	0.060805923
111	0.356443	0.069255	0.385068117	0.072392438	0.363919685	0.067066822
112	0.358779	0.069159	0.335249553	0.070284202	0.287288216	0.069686866
113	0.35813	0.069043	0.281261148	0.071106484	0.448714813	0.064516709
114	0.332362	0.0689825	0.254569782	0.066132833	0.282899346	0.064583463
115	0.292908	0.068975	0.333257581	0.065682773	0.264091535	0.075918534
116	0.28877	0.06899	0.318198002	0.058662544	0.247712099	0.065414868
117	0.2579605	0.069038	0.250782517	0.066808829	0.406460805	0.066517684
118	0.208236	0.069132	0.203994424	0.067864553	0.079783388	0.065293253
119	0.187885	0.069257	0.185166644	0.071262513	0.190221845	0.060742571
120	0.1630905	0.069377	0.17680974			

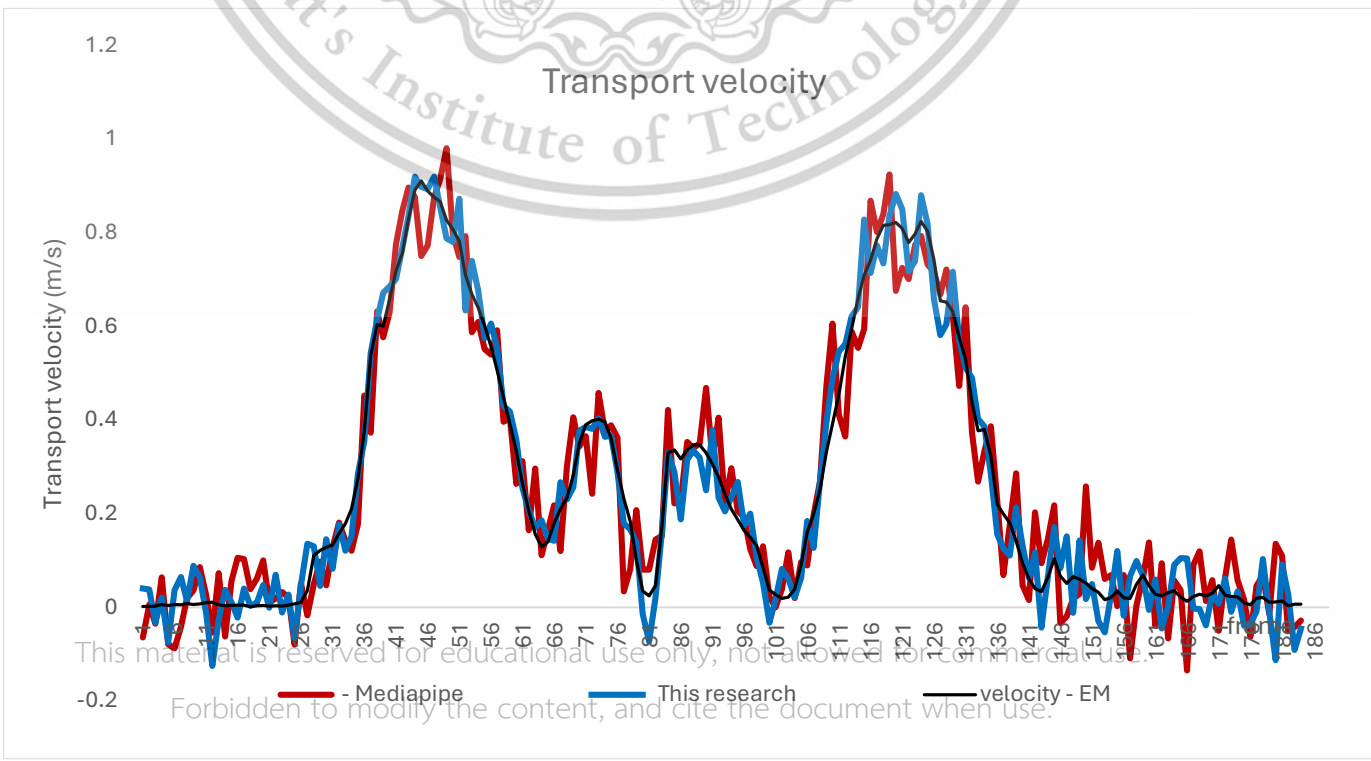
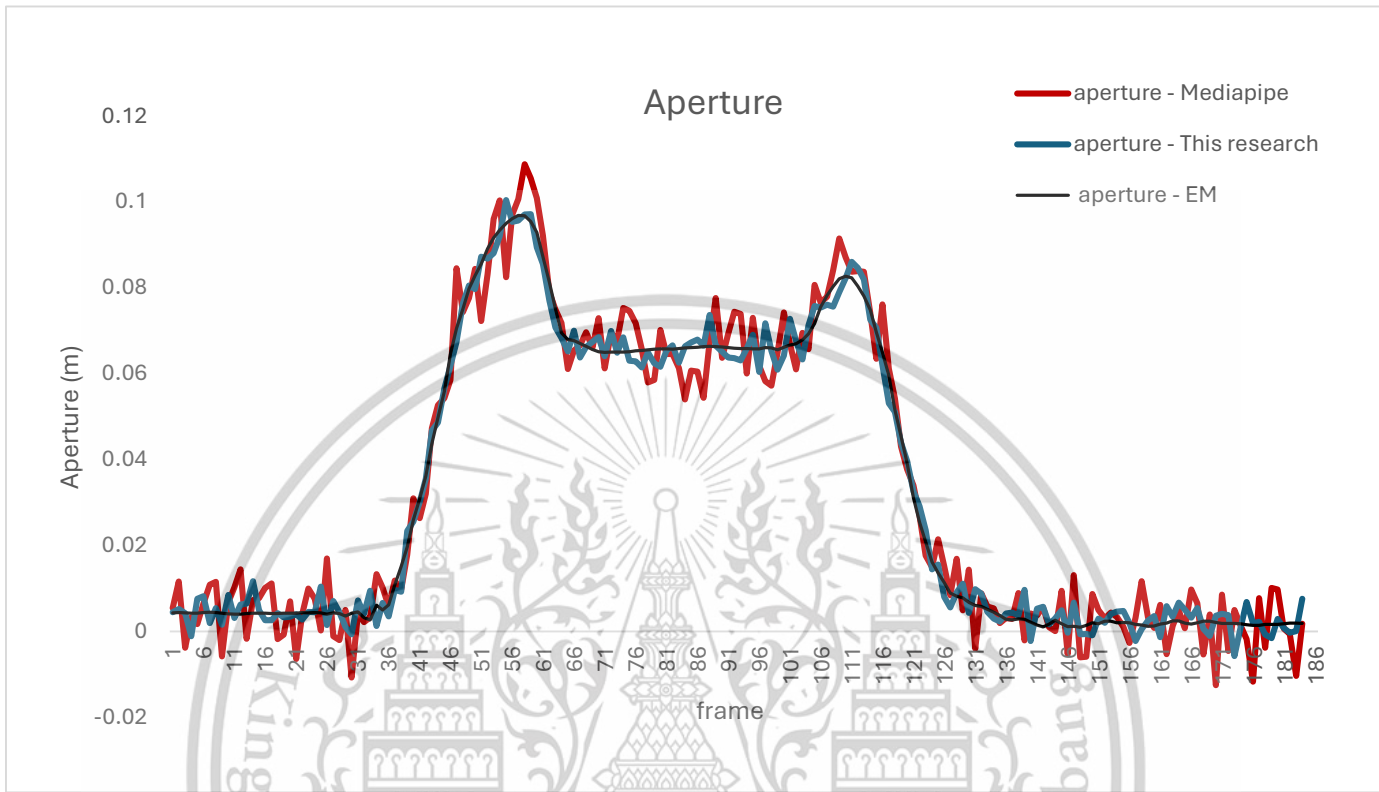


This material is reserved for educational use only, not allowed for commercial use.

Forbidden to modify the content, and cite the document when use.

Table 5 Result from trial5

frame	velocity - EM	aperture - EM	This research	aperture - This research	- Mediapipe	aperture - Mediapipe
1	0.001649	0.0043175	0.039838827	0.004458098	-0.064306633	0.005416207
2	0.002027	0.004365	0.038292238	0.005234395	0.005786515	0.011636615
3	0.0020905	0.004343	-0.032963519	0.004234879	-0.035455146	-0.003834034
4	0.005832	0.0042565	0.020829356	-0.001164479	0.06433354	0.00329344
5	0.004098	0.004263	-0.075776044	0.007583058	-0.079320558	0.001715223
6	0.0055985	0.004398	0.03641816	0.008192801	-0.088187032	0.006499208
7	0.005235	0.00446	0.064659036	0.001953073	-0.041790154	0.010867103
8	0.00757	0.00436	0.01329636	0.005399424	0.019792584	0.011562153
9	0.006107	0.0042605	0.08894155	0.001560739	0.035609428	-0.005852997
10	0.007374	0.004091	0.064063448	0.008486065	0.085690207	0.00678121
11	0.009947	0.003981	-0.013951903	0.003141295	0.02493989	0.010311663
12	0.010577	0.0039935	-0.125368445	0.00625587	-0.05465291	0.014498912
13	0.005293	0.004128	-0.026359039	0.006442791	0.07265195	-0.001726116
14	0.003247	0.004209	0.036991674	0.011735663	-0.062471113	0.007268162
15	0.0034505	0.0042345	0.010951322	0.004866555	0.056467417	0.007775693
16	0.004502	0.0042085	-0.022090952	0.002619563	0.105988114	0.010139918
17	0.004175	0.004181	0.040386884	0.002620958	0.102858638	0.011197798
18	0.001423	0.004188	0.003277765	0.004222847	0.038401126	-0.001782338
19	0.003019	0.0042015	0.009213601	0.003249642	0.060353601	-0.000778438
20	0.004128	0.004206	0.047850773	0.003380297	0.100500297	0.007034467
21	0.002112	0.004272	-0.000898883	0.004020583	0.00960585	-0.006403748
22	0.00327	0.004368	0.069570578	0.002753833	0.01893758	0.004112409
23	0.002542	0.004329	-0.011565108	0.004565951	-0.032619447	0.009976155
24	0.004204	0.004411	0.026837349	0.004449922	0.020649277	0.007624532
25	0.0073325	0.004275	-0.066974867	0.010454971	-0.079665752	0.00021226
26	0.010826	0.004046	0.047691847	0.001472302	0.050720333	0.016987932
27	0.035531	0.004282	0.135784716	0.007066519	-0.017526069	-0.001151725
28	0.110565	0.004157	0.130290081	0.004424878	0.048802609	-0.002021983
29	0.121566	0.003566	0.045837123	0.00100664	0.097837371	0.004951169
30	0.128447	0.004222	0.145125943	-0.000680583	0.047208126	-0.010769814
31	0.133419	0.004525	0.082192602	0.007252623	0.128396533	0.004487303
32	0.157448	0.003172	0.177350511	0.004088902	0.180897483	0.002115106
33	0.178859	0.0026395	0.120610917	0.009492128	0.142117343	0.003236272
34	0.210599	0.006077	0.151483034	0.001258625	0.120729126	0.013328204
35	0.274803	0.004995	0.285209735	0.006652384	0.17661746	0.010194264
36	0.3766135	0.00619	0.355685063	0.003491158	0.452828924	0.005828321
37	0.5390635	0.010833	0.543659566	0.009652246	0.373556764	0.011866043
38	0.60468	0.015109	0.614731202	0.009216116	0.63241653	0.009693001
39	0.600771	0.019695	0.67195457	0.02343909	0.577143861	0.017881771
40	0.658486	0.0259745	0.685666959	0.025613834	0.630729997	0.03103614
41	0.719726	0.030971	0.701628322	0.03010943	0.776497707	0.026437232
42	0.757339	0.0362045	0.769040333	0.035607265	0.847946662	0.032102607
43	0.829478	0.043766	0.836254132	0.046812141	0.897154202	0.047116767
44	0.891523	0.049824	0.920470795	0.048697118	0.877722673	0.052758081
45	0.9120015	0.05598	0.898835556	0.056641958	0.751007325	0.054431469
46	0.889827	0.0647115	0.893868056	0.061944892	0.773714406	0.058652882
47	0.877086	0.070692	0.920788811	0.0675593	0.875867139	0.08472371
48	0.867095	0.0752605	0.858480003	0.076488778	0.914799956	0.074465726
49	0.827684	0.07996	0.788453148	0.080655377	0.982092781	0.077749302
50	0.807492	0.082969	0.780968801	0.079828883	0.797040327	0.084587609
51	0.782088	0.085672	0.873477462	0.087374023	0.748591465	0.072422564
52	0.710408	0.0892885	0.634384816	0.086978507	0.793164812	0.083283242
53	0.669177	0.091815	0.740894635	0.088211188	0.588373366	0.09619649
54	0.6400115	0.093582	0.676944028	0.09213644	0.610196638	0.100533063
55	0.60167	0.0951825	0.575241724	0.100628861	0.551891785	0.082590144
56	0.55735	0.096248	0.606569738	0.095512412	0.54010846	0.097166244
57	0.50632	0.097075	0.554017761	0.095797771	0.592452389	0.100842411
58	0.448156	0.096913	0.42989098	0.097262943	0.396494227	0.108975445
59	0.391471	0.09564	0.418486405	0.097342323	0.404400256	0.105682469
60	0.3336095	0.093051	0.358434922	0.089580569	0.263441246	0.101050464
61	0.2654135	0.087397	0.255500786	0.085698721	0.21121239	0.092345971
62	0.205855	0.081478	0.206232568	0.077229072	0.164655042	0.079207372
63	0.156276	0.075331	0.169784651	0.070859034	0.296576427	0.075106907
64	0.129162	0.069649	0.18604947	0.068435336	0.111156996	0.071970587
65	0.139944	0.068053	0.146829877	0.065308856	0.165813185	0.061155242
66	0.1799405	0.06786	0.141803447	0.070113617	0.217699723	0.065517816
67	0.2105985	0.067197	0.266945365	0.063860421	0.119810552	0.066748222
68	0.233797	0.066482	0.230497074	0.066379414	0.299979419	0.069811604
69	0.282143	0.065781	0.256035209	0.067573395	0.406237996	0.066163001
70	0.350505	0.0652095	0.37706918	0.068666926	0.343916138	0.073087358
71	0.39009	0.065092	0.385890328	0.064147988	0.365430049	0.061334419
72	0.3983115	0.065114	0.381761142	0.070047551	0.242318628	0.069670876
73	0.40214	0.065117	0.404248808	0.065005975	0.458264297	0.067807589
74	0.396259	0.065125	0.364140482	0.068582012	0.375199412	0.075450845
75	0.3620215	0.065285	0.366860164	0.063128047	0.388825005	0.074765815
76	0.2932115	0.065432	0.289523201	0.062972466	0.363006341	0.071836466
77	0.232349	0.065553	0.288798867	0.06156731	0.033573295	0.065949315
78	0.1834755	0.0656875	0.166858573	0.065108636	0.081937206	0.058048087
79	0.1066085	0.065819	0.13957301	0.062511332	0.207893959	0.058620895
80	0.034358	0.065897	-0.014442595	0.061717221	0.080420693	0.070329398
81	0.024219	0.06586	-0.073840838	0.065471764	0.080125906	0.064707653
82	0.045925	0.065789	0.020632686	0.066692689	0.144843745	0.064669536
83	0.172477	0.065939	0.161437498	0.062721173	0.15208598	0.061410592
84	0.3302735	0.0661515	0.32980018	0.066518785	0.421945711	0.054102526
85	0.336396	0.0661915	0.288798867	0.067371218	0.221876068	0.060805476
86	0.316903	0.066299	0.187699041	0.068022536	0.228027641	0.060576406
87	0.336153	0.066452	0.315674114	0.066633946	0.353566391	0.054489496
88	0.347455	0.066479	0.288798867	0.073831691	0.340095939	0.067581354
89	0.347357	0.06639	0.320102653	0.066604669	0.350190083	0.077748665
90	0.329765	0.066305	0.2498632	0.065193799	0.469284754	0.063833711
91	0.305569	0.0661685	0.379012522	0.063881986	0.316711825	0.069372641
92	0.279066	0.066061	0.234491545	0.066061	0.234491545	0.063725273
93	0.2415625	0.0659945	0.204959586	0.0659945	0.204959586	0.063228263
94	0.2095415	0.065936	0.234760917	0.065936	0.234760917	0.065947979
95	0.187199	0.065887	0.267539461	0.065887	0.267539461	0.069202903
96	0.163934	0.065891	0.174880345	0.065891	0.174880345	0.060557305
97	0.1495175	0.0662265	0.199890276	0.0662265	0.199890276	0.071883307
98	0.131741	0.066139	0.107311471	0.066139	0.107311471	0.065435959
99	0.0842235	0.0665705	0.052529032	0.0665705	0.052529032	0.06105358
100	0.036581	0.0662455	0.033451293	0.0662455	0.033451293	0.064332201
101	0.02674	0.066778	0.016635203	0.066778	0.016635203	0.072911771
102	0.019163	0.067064	0.081783891	0.067064	0.081783891	0.067788903
103	0.0213395	0.0679605	0.061321768	0.0679605	0.061321768	0.063444524
104	0.038875	0.069377	0.020810979	0.069377	0.020810979	0.071398109
105	0.0904225	0.071775	0.062780795	0.071775	0.062780795	0.075916498
106	0.160658	0.075643	0.184685607	0.075643	0.184685607	0.075531914
107	0.199244	0.078367	0.126639379	0.078367	0.126639379	0.07622833
108	0.251694	0.0804455	0.269166447	0.0804455	0.269166447	0.075776503
109	0.332192	0.0822275	0.395090112	0.0822275	0.395090112	0.079099741
110	0.391503	0.082824	0.488051301	0.082824	0.488051301	0.082368864
111	0.4547105	0.0824615	0.546871601	0.0824615	0.546871601	0.086166788
112	0.535848	0.0805595	0.561843636	0.0805595	0.561843636	0.084777836
113	0.596453	0.078219	0.622485568	0.078219	0.622485568	0.082101498
114	0.6599055	0.0749985	0.64241196	0.0749985	0.64241196	0.072671599
115	0.709867	0.069746	0.82886805	0.069746	0.82886805	0.070789908
116	0.741947	0.065106	0.714934738	0.065106	0.714934738	0.062062462
117	0.7879205	0.05967	0.773416273	0.05967	0.773416273	0.053182553
118	0.816602	0.0516195	0.735218239	0.0516195	0.735218239	0.051215808
119	0.818074	0.04548	0.836560157	0.04548	0.836560157	0.043899663
120	0.822762	0.0393215	0.883368575	0.0393215	0.883368575	0.039803742
121	0.8099395	0.031127	0.850715			



BIOGRAPHY

Name: Mr. Sahawatchara Thongprasan
Date of Birth: November 24, 1994, in Nakhonsawan
Address: Nakhonsawan 60000

Educational Background:

2018: Bachelor of Engineering in Chemical Engineering ,
King Mongkut's Institute of Technology Ladkrabang.

